Open Access Research Journal of
Life Sciences
Journals home page: https://oarjpublication/journals/oarjls/
ISSN: 2783-025X (Online)

OARJ OPEN ACCESS RESEARCH JOURNALS

(RESEARCH ARTICLE)

Check for updates

Multifractal structure of acini immunoreactive to cytokeratin 18 in normal and pathologic prostate

Luis Santamaría [1,*], Ildefonso Ingelmo [2] and Fernando Teba [3]

[1] *Department of Anatomy, Histology, and Neuroscience. School of Medicine, Autonomous University of Madrid. C/Arzobispo Morcillo 2, 28029-Madrid, Spain.*
[2] *Department of Anaesthesiology. Hospital Ramón y Cajal, Madrid, Spain.*
[3] *Department of Surgery (Urology). Hospital de La Princesa, School of Medicine, Autonomous University of Madrid, Spain.*

Open Access Research Journal of Life Sciences, 2026, 11(01), 009-033

Publication history: Received on 31 December 2025; revised on 07 February 2026; accepted on 09 February 2026

Article DOI: https://doi.org/10.53022/oarjls.2026.11.1.0036

Abstract

As with other biological textures, the complexity of the distribution of acini from the prostate could be characterized by fractal geometry. In the present study the fractality of prostatic acini immunoreactive for cytokeratin 18 (ck18) in normal prostate (CTR), benign prostatic hyperplasia (BPH), and adenocarcinoma (CA) will be analyzed to detect fractal changes in BPH and CA about CTR. Other texture parameters such as lacunarity (Λ) and the local connected fractal dimension (LCFD) were also estimated. Specimens from all the groups were immunostained to ck18 and studied by multifractal analysis, calculating the multifractal spectrum f(α), and the generalized dimension D_Q. LCFD and Λ were estimated to assess the heterogeneity of acinar distribution. To find out if the random distribution of immunostaining for ck18 produces changes in the fractality of the cases studied, the same analysis methods were applied to the surrogate data obtained from the real data. Principal Components Analysis (PCA) was used to find patterns or groupings of the CTR, BPH, and CA cases. The results suggest that the acinar distribution shows a multifractal structure in both normal and pathological prostate. The degree of multifractality in CA is significantly higher than in CTR and BPH. It is also observed that the heterogeneity of the acinar structure of the CA is greater than in CTR and BPH, as indicated by lacunarity and LCFD. The variables introduced in the PCA discriminate the CA group from the CTR and BPH groups.

Keywords: Prostate Cancer; Benign Prostate Hyperplasia; Multifractals; Generalized Fractal Dimension; Lacunarity; Surrogate Data

1 Introduction

The two most common pathological conditions in the human prostate are benign prostatic hyperplasia (BPH) and prostatic adenocarcinoma (CA). It is well known that both pathologies are androgen-dependent and involve abnormal proliferation of the prostatic epithelium and the participation of the stroma in the pathogenesis of both conditions, however, BPH cannot be considered as the benign variant of a prostatic tumor growth whose malignant variant is adenocarcinoma. Benign prostate hyperplasia (BPH) is the most common benign disease of the human prostate (*Barry MJ 1990; Kirby RS 1992*), representing approximately 50% of medical consultations made by urological disease (*Birkhoff JD 1983; Burgos Rodríguez R and Chicharro Molero JA 1993*). Although the pathogenesis of BPH is unclear, it is known to be multifactorial; being necessary for the presence of two factors for prostate growth: the androgen stimulus and age (*Isaacs JT 1994*). Different theories have been proposed, based on histological, and hormonal age-related changes, but, currently, not a single explanation is accepted (*Oesterling JE 1991*). Androgens possibly act as initiators of stromal hyperplasia, which induces epithelial hyperplasia (*Berry SJ, et al. 1984; Fitzpatrick JM 2006*). Prostate adenocarcinoma is a complex system consisting of different cell clones that interact with each other and with normal cells. These sorts of interactions are the frequent cause of intratumor heterogeneity that is observed at different stages of tumor progression, metastasis, and recurrence (*Park Y, et al. 2016*). Although prostate carcinoma remains one of the most

* Corresponding author: Luis Santamaría

common carcinomas affecting the male population, little is known about the variability of local changes in the expression of different markers and their relationship with the behavior of the tumor.

In both BPH and CA, the expression of cytokeratin in epithelial cells can manifest various alterations. The cytokeratin class of intermediate filaments has been shown to exist in all epithelia (*Franke WW, et al. 1979*). There are now recognized 19 distinct cytokeratins expressed in human epithelia, and each epithelial type has a different phenotype concerning these proteins (*Moll R, et al. 1982; Quinlan RA, et al. 1985*). Early studies using polyclonal anti-cytokeratins demonstrated that the basal cells of the prostate have cytokeratins that show different immunoreactivities from the luminal or columnar cells (*Schlegel R, et al. 1980; Barwick K and Mardi A 1983*). Several studies using monoclonal anti-cytokeratin antibodies have differentiated the columnar and basal cell populations by their specific cytokeratin content (*Brawer MK, et al. 1985*). The columnar cells react with monoclonal antibodies to cytokeratin 18 (ck18) (*Nagle RB, et al. 1987*). Besides, chemical determination of the cytokeratin phenotype of three established human prostatic carcinoma cell lines also suggests that all three cell lines synthesize ck18 (*Nagle RB, et al. 1987*). When comparing the immunoexpression of ck18 in BPH with normal prostate, no remarkable differences are detected (*Nagle RB, et al. 1987; Verhagen AP, et al. 1992*). Nevertheless, the percentage of positivity for luminal ck18 was statistically lower for BPH cultures concerning the positivity observed for both prostatic intraepithelial neoplasia (PIN) and prostate adenocarcinoma-derived cultures (*Festuccia C, et al. 2005*). The distribution of cytokeratin 18 (ck18) immunoexpression has been studied in both BPH and CA. The findings described by some authors (*Santamaría L, et al. 2017*) indicate that changes in the expression of ck18 in BPH are not homogeneous, besides, the local changes in the expression of ck18 are more evident in terms of volume fraction of ck18 (V_V ck18) and its local variability, whereas other parameters that are useful in other pathologies, such as lacunarity, are less relevant in BPH. Likewise, studies of ck18 expression in prostatic adenocarcinoma (*Santamaria L, et al. 2018*) indicate that changes in the expression of ck18 by the cancer prostate are heterogeneous. The increase in local variability of ck18 immunoexpression can be related to the increase in heterogeneity of the shape and size of the tumor acini. The symmetry of the distribution of the local values of V_V ck18 along the axis of the space series may indicate the existence of anisotropy in the distribution of tumor acini. The increase in scale-dependent entropy for V_V ck18 in cancer (*Santamaria L, et al. 2018*) at the morphological level could be interpreted as the macroscopic expression of the same increase at the molecular level already described (*Humphrey PA 2004; Iczkowski KA, et al. 2011; Tolkach Y and Kristiansen G 2018*). As with other biological textures (*Landini G and Rippin JW 1993; Losa GA and Nonnenmacher TF 1996; Sedivy R and Windischberger C 1998; Sijilmassi Q, et al. 2020*), the complexity of branching and distribution of acini immunoreactive for ck18 from both BPH and CA could be characterized by fractal geometry and such geometry could be related to a nonlinear deterministic dynamic underlying the processes of acinar growth and development. In addition, the complexity of the distribution of prostate acini likely extends through different scales since there are different sizes and orders of branching (*Santamaría L, et al. 2016*); therefore, it is likely that the fractal dimension is not unique but that we are dealing with a multifractal structure (*Ivanov PC, et al. 1999; Reljin IS and Reljin BD 2002*). Recently, many physical quantities that do not obey conventional scaling laws have been considered. Broad probability distributions are characteristic of such observables. In all cases, the moments of the distributions cannot be characterized by a single exponent. An infinity hierarchy of exponents is required. This phenomenon was described for the first time by B. B. Mandelbrot in the context of fully developed turbulence (*Mandelbrot BB 1974*); today, it is known by the neologism multifractality. A brief description of the concept of fractal dimension and its various types is indicated in another publication (*Santamaria L and Ingelmo I 2023*). In addition to the possible establishment of the fractal or multifractal character of the distribution of immunoreactivity for ck18 of the prostate epithelium, it may be interesting to find out if pathological alterations, whether benign (BPH) or malignant (CA), show changes in the fractality of the immunoreactive acini, as described in other organs or systems in situations such as aging (*Goldberger AL, et al. 2002*), the action of toxic products (*Manera M, et al. 2013*), various pathologies (*Atupelage C, et al. 2012*), etc. The complexity of the distribution of prostate acini immunoreactive to ck18 suggests that its structural pattern may exhibit multiple scaling rules rather than a single global scale. That is, the study of epithelial cells positive to ck18 either in normal prostate (CTR), benign prostatic hyperplasia (BPH), or prostatic adenocarcinoma (CA) could be approached through multifractal analysis. Therefore, in the present work, the distribution of epithelial cells immunostained for ck18, in the three study groups (CTR, BPH, and CA) will be analyzed for the possible detection of their multifractal structure, calculating several types of multifractal spectra. The fractal dimension is not a complete identifier of the texture of the tissue, so other concepts have been proposed to distinguish between structures that have the same fractal dimension but look different (*Sijilmassi Q, et al. 2020*). The Lacunarity (Λ), a multiscale analytical measure that evaluates tissue heterogeneity will be applied in the three study groups. On the other hand, the cell population that expresses ck18 is subject to local variations in the conditions of their development, so their fractal characteristics change from one point to another (*Karperien A, et al. 2008*). For this purpose, local measures of fractality have been developed and tested in various types of biological tissues as a comparison between normal and pathological tissues (*Landini G, et al. 1995; Landini G and Rippin JW 1996; Losa GA and Nonnenmacher TF 1996; Karperien A, et al. 2008*); in the present work, the application of these local measurements of fractality through the analysis of the Local Connected Fractal Dimension (LCFD) (*Sijilmassi Q, et al. 2020*) will be carried out. To find out if

the random distribution of immunostaining for ck18 produces changes in the fractal structure of the cases studied, the same methods of analysis of fractal dimensions, multifractality, and lacunarity were applied to the surrogate data obtained from the real data in CTR, BPH and CA (*Spasic S, et al. 2011*).

Summarizing, in the present study the fractality of prostatic acini immunoreactive for ck18 in normal prostate (CTR), benign prostatic hyperplasia (BPH), and prostatic adenocarcinoma (CA) will be analyzed to detect possible fractal changes in BPH and CA about CTR. In addition, other texture parameters such as lacunarity and the local connected fractal dimension will be studied in the three groups.

2 Material and Methods

2.1 Material

Thirty prostate specimens were collected over one year (2015-16), at La Princesa Hospital (Madrid, Spain), 10 were from adults, (CTR group), age (mean ± SD): 45 ± 7; range: 30 - 47 years, all these specimens were of healthy subjects, without endocrine or reproductive pathology, deceased in traffic accidents, and eligible as donors for transplant, the age of the subjects of CTR group was in the range indicated to avoid any histological changes of subclinical BPH, relatively frequents in subjects older than 50 years, 10 were surgical specimens (adenomectomies) from patients diagnosed of the adenofibromiomatous type of benign prostatic hyperplasia, (BPH group), age (mean ± SD): 75 ± 10, Range: 65 - 85 years. The other 10 were surgical specimens (radical prostatectomy) from patients diagnosed with prostate carcinoma (CA group): age (mean ± SD): 70±10, range: 56 to 85 years. In all these cases, the diagnosis of carcinoma was previously confirmed by histopathology. The cancer cases were graded according to the Gleason score (Epstein et al., 2005) and the average grading was 7 (3+4). All of these cases were without prior neoadjuvant hormonal therapy. All the ethical requirements were accomplished to obtain the prostatic tissue either at the moment of the multiorganic extraction for transplant (CTR) or at the surgery (BPH and CA).

2.2 Processing of the Tissues

Immediately after extraction, the specimens were fixed for a week in 10% paraformaldehyde in PBS, pH 7.4. After fixation, the specimens from the three groups were thoroughly sectioned into 2-mm-thick slices, performed by isotropic uniform random sampling (IUR sections) to preserve the isotropy of the tissue (*Odgaard A and Gundersen HJ 1993*). The specimens were processed for paraffin embedding. The paraffin blocks were exhaustively sectioned, 20 sections (5-µm-thick) were performed on each block for immunostaining.

2.3 Immunohistochemistry

At least five randomly selected slides per specimen were immunostained for ck18 in CTR, BPH, and CA groups. Deparaffinized and rehydrated tissue sections were treated at room temperature for 30 min with hydrogen peroxide 0.3% in phosphate-buffered saline (PBS) pH 7.4, to block endogenous peroxidase. To detect ck18 immunoreactivity, sections were incubated with a monoclonal anti-cytokeratin-18 antibody (Abcam, Cambridge, UK) diluted at 1:250. Pretreatment of sections by heat in citrate buffer pH 6.0 (using a pressure cooker) (*Martin JJ, et al. 2001*) was performed to enhance immunostaining. The primary antiserum was diluted in PBS pH 7.4 containing 1% bovine serum albumin (BSA) (Sigma, St Louis, USA) plus 0.1% sodium azide (Merck, Darmstadt, Germany). The incubation with primary antiserum was overnight at 4ºC. The second antibody employed was a biotin-caproyl-anti-rabbit immunoglobulin (Biomeda, Foster City, CA, USA). The second antibody was diluted at 1/400 in PBS containing 1% BSA without sodium azide and incubated for 30 min at room temperature. Thereafter, sections were incubated with a streptavidin-botin-peroxidase complex (Biomeda). The immunostaining reaction product was developed using 0.1 g diaminobenzidine (DAB) (Sigma) in 200 mL of PBS, plus 40 µL hydrogen peroxide. After immunoreaction, nuclear counterstaining with Harris hematoxylin was performed in some sections. No nuclear counter-staining was performed on the remaining sections that were then employed for quantitative purposes. All slides were dehydrated in ethanol and mounted in a synthetic resin (Depex, Serva, Heidelberg, Germany). The specificity of the immunohistochemical procedures was checked by incubation of sections with no immune serum instead of the primary antibody.

2.4 Data Acquisition

The acquisition of the data used was carried out in a similar way to that described in other studies (*Santamaría L, et al. 2017; Santamaria L, et al. 2018; Santamaria L and Ingelmo I 2023*). For multifractal analysis, 5 strips of an average of 20 immediately adjacent quadrats (range 10-40) were explored for each immunostained section from CTR, BPH, and CA groups. The origin and sense of the axis for each strip were chosen by systematic random sampling (*Sorensen FB 1991*) for all the strips. The result was a series of images from all the groups, sized, on average, 512 X 7000 pixels. For

lacunarity and LCFD measurements, 5 additional fields sized 512 X 700 pixels were selected by systematic random sampling for each immunostained section from CTR, BPH, and CA groups. In all cases (strips and additional fields), the final magnification (X100) was such that 512 pixels represented 655 μm. At that point, the strips were 9 mm long, on average. Therefore, the total length explored per section (five sections) and per case (10 cases) was 9 X 5 X 10 = 450 mm (for BPH and CA cases, an appreciable percentage of the maximum specimen diameter) (*Baddeley A and Vedel Jensen E 2005*). The images were captured using a color digital camera DP 70 (Olympus Corporation of the Americas, PA, USA) with a resolution of 12.5 megapixels, attached to an Olympus microscope fitted with a motorized stage controlled by the stereological software Cast-Grid (Stereology Software Package, Silkeborg, Denmark). This program controls the XY displacement of the microscope stage and allows the selection of fields to be studied by random systematic sampling after the input of an appropriate sampling fraction (*Arriazu R, et al. 2005*). The strips were then mounted from the quadrats captured, using the public domain Java image processing program, Image J (version 1.48), developed at the US National Institutes of Health and available on the Internet at https://imagej.net/ (*Rasband WS 2012*). Subsequently, the resultant strips and additional fields were processed using the same software. A binary image was produced where the immunostaining to ck18 was shown as black and the pore space (lumina of acini, stroma, etc.) as white (Figures 1 a-f). To explore whether the random distribution of immunostaining for ck18 produces changes in the fractal structure of the tissues, surrogates were generated from the strips and the fields obtained, a transformation was applied to each image that causes the shuffling of the immunostained pixels, producing the randomization of the visualized tissues (Figure 1 g).

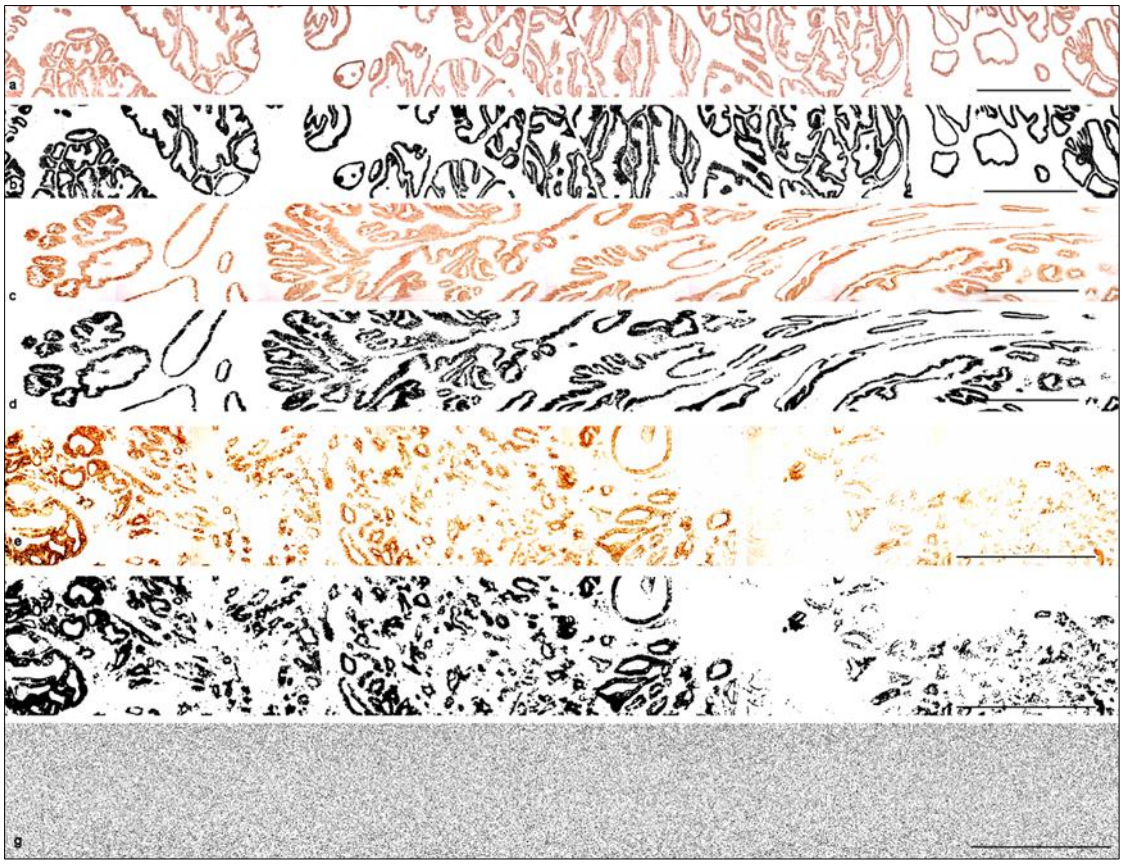

Figure 1 In (a) the image shown is a strip from a specimen of CTR group immunostained to ck18; in (b) the image from (a) was processed to segment the immunostained acini; the image from (c) represents a strip from a specimen of BPH group also immunostained to ck18; the image from (d) shows the processing and segmentation of image (c); in (e) the image shown is a strip from a specimen of CA group immunostained to ck18; in (f) the image from (e) was processed to segment the immunostained acini. In (a) the binarized image shown is a strip from a specimen of the CA group immunostained to ck18; in (g) the image represents the surrogate data generated from image (f). In all the images, the scale bars represent 224 μm

This operation was carried out by applying the ComsystanJ plugin contained in the Image J software. Five surrogates were produced from each real image obtained in the three study groups. Both real and surrogate images were stored in jpg format.

2.5 Quantitative measurements

2.5.1 Volume fraction of immunostained epithelium

To obtain an overview of the relative magnitude of immunostaining for ck18, measurements of the fraction of the volume of tissue immunostained to ck18 (V_V ck18) were made. In each image, the fraction of pixels belonging to the immunostained epithelium expressed as a percentage over the space of reference (pore space plus immunoreactive epithelial component) was automatically recorded by the image analysis system for each image in each case for the CTR, BPH, and CA groups.

2.5.2 Multifractal parameters

A more detailed explanation of the concept and meaning of the different multifractal parameters has been given elsewhere (*Santamaria L and Ingelmo I 2023*). The software for the estimation of multifractal parameters included in the FracLac plugging from Image J software (version 1.48) was applied in all of the binarized images from each case studied. FracLac generates a mass distribution for a binarized image; from this, a spectrum of values for the generalized dimension (D_Q) is calculated. D_Q addresses how mass varies with an image's ε (resolution or box size). This is done using graphs known as multifractal spectra, one practical multifractal spectrum is the graph of D_Q vs Q, where D_Q is the generalized dimension for a dataset, and Q is an arbitrary set of exponents. The expression generalized dimension thus refers to a set of dimensions for a dataset. The general pattern of the graph of D_Q vs Q can be used to assess the scaling in a pattern. The graph generally decreases and is sigmoidal around Q = 0, where $D_0 \geq D_1 \geq D_2$. The generalized dimension also gives important specific information. D_0 is equal to the capacity dimension (box counting dimension). D_1 is equal to the information dimension, and D_2 is equal to the correlation dimension. Multifractals have multiple dimensions in the D_Q versus Q spectra, but monofractals stay relatively flat in that area. Another useful multifractal spectrum is the f(α) graph over a range of diverging exponents α (*Santamaria L and Ingelmo I 2023*). This graph generally rises to a maximum approximating the fractal dimension at Q = 0 and then falls. Like D_Q versus Q spectra, f(α) shows typical patterns for comparing non-, mono-, and multifractal patterns. In particular, non- and mono-fractals converge on specific values for this spectrum, whereas the spectrum from multifractal patterns typically forms humps over a broader area.

In summary, on the binarized images, the following estimates were performed:

2.5.3 Multifractal spectrum f(α) versus α.

Measurement of the degree of multifractality. In the graph f(α) vs α, Δα is the difference between the maximum and minimum α when f(α) > 0, ($\Delta\alpha = \alpha_{max} - \alpha_{min}$), Δα makes a quantitative measurement of the degree of multifractality, the broader the Δα, the stronger the multifractality, and the richer and more complex the image pixel intensity distribution is (*Hu MG, et al. 2009*). Asymmetry of the f(α) spectrum shape is also an important index of multifractality. It indicates the degree of fluctuation in different fractal exponents (*Hu MG, et al. 2009*). A left-skewed spectrum denotes high fractal exponents and large fluctuations dominate the measure, while a right-skewed spectrum implies low fractal exponents and low fluctuations are dominant. To estimate the skewness quantitatively, the degree of asymmetry was calculated with the formula:

$$A = \frac{(\alpha_0 - \alpha_{min})}{(\alpha_{max} - \alpha_0)}$$

Where A = 1 if the spectrum is symmetric and A > 1 or A < 1 when the spectrum is left-skewed or right-skewed (*Szczepaniak A and Macek WM 2008*).

2.5.4 Generalized dimension D_Q versus Q.

From the D_Q vs Q graph, the dimensions D_0 (capacity dimension), D_1 (information dimension), and D_2 (correlation dimension) were extracted.

Each value of Q is an exponent used in calculating the multifractal spectra. The maximum, minimum, and increment between Qs are arbitrary values the user sets; the range employed was from -10 to 10, incremented by 0.1. All these measurements were carried out on each case's real and surrogate images, obtaining at the end graphs in which the mean of each estimator ± CI (95%) was expressed.

2.5.5 Local connected fractal dimension analysis

There are several parameters associated with a local fractal dimension (*Sijilmassi O, et al. 2020*). In the present work, we will adopt the local connected fractal dimension (LCFD) that was calculated using the plugin FracLac (*Voss RF and Wyatt JCY 1993; Landini G, et al. 1995*). To measure LCFD, only the number of pixels (P) from the image that are connected were taken into account. P varies with the scale ε as $N_C(\varepsilon) \approx F_C \varepsilon^{D_C}$ where F_C is a prefactor, and D_C the LCFD. LCFD measurements were carried out on each case's real and surrogate images. In each group, the histogram of the frequency of the distribution of LCFD was carried out, both in real and surrogate cases.

2.5.6 Lacunarity

The fractal dimensions are not a complete identifier of the texture of the tissue (*Sijilmassi Q, et al. 2020*), so other concepts have been proposed to distinguish between structures that have the same fractal dimensions but look different. One of these concepts is lacunarity (Λ). It is a multiscale analytical measure that evaluates tissue heterogeneity. It has been defined as the degree of gappiness, heterogeneity, and translational and rotational invariance in an image (*Bartsch G 1977; Teba F, et al. 2007*). Generally, is it used to determine the texture associated with patterns of spatial dispersion (*Howard CV and Reed MG 1998; Patel ND and Parsons JK 2014*). The lacunarity was estimated by the sliding box method, implemented by the FracLac plugin. As lacunarity depends on the scale ε, in addition to obtaining a global estimate of Λ for each case, graphs of Λ vs ε were drawn both in real and surrogate cases.

All quantitative estimates (V_V ck18, Δα, A, D_0, D_1, D_2, LCFD, Λ) were expressed as mean ± CI (95%) for each group of study (CTR, BPH, and CA) in both real and surrogated data. The Student t-test was applied to compare the real data with the surrogate data in all groups. For the comparison between the three study groups in real and surrogate data respectively, ANOVA was used, comparing the means of each group using the Tukey test, the level of significance was $p < 0.05$.

2.5.7 Principal components analysis

In general terms, principal components analysis (PCA) is a useful statistical technique for finding patterns in data of high dimension (*Sijilmassi O, et al. 2020*), for this reason, it is often used in biological and medical image analysis (*Arriazu R, et al. 2005*). PCA allows a large number of possibly correlated quantitative variables to be reduced to a smaller number of transformed variables (principal components) that explain much of the variability in the data. In this study, PCA will be applied to find patterns or groupings of the cases by representing the first two principal components. It could be interesting to observe if the clustering defined by PCA coincides with the groups studied, that is if the variables introduced in the analysis are capable of structuring the cases according to their allocation in CTR, BPH, or CA groups. The quantitative variables introduced in PCA were: Local connected fractal dimension (LCFD); Degree of multifractality (Δα); Asymmetry of f(α) spectrum (A); Capacity dimension (D_0); Correlation dimension (D_2); Lacunarity (Λ). Of the 6 principal components obtained, the first two (PC1, and PC2) that explain more than 70% of the variance were selected. The method used for selection was Horn's parallel analysis (*Horn JL 1965*).

To visualize the results of PCA, the next graphs were generated:

- Proportion of variance plot, it expresses the proportion of variance explained by each PC.
- Loadings plot, that represents the numerical values from the loading's matrix of the specified principal components, providing information useful for identifying clusters of variables.
- PC score used to plot the data along the chosen principal component axes, this graph is useful for visualizing clustering, based on where certain points appear about the others along the two selected components.

PCA was performed on both the real data and the surrogate data sets. To find out if there are differences between the distribution of points in the PC score of the real data compared to that of the surrogate data, a contingency analysis was used using the Chi^2 test. GraphPad Prism 9 (GraphPad software, MA, USA) was used to carry out all the statistical studies and graphs.

3 Results

3.1 Volume fractions of immunostained epithelium

As shown in Figure 2a, no significant differences were observed for V_V ck18 when comparing the results of the three groups studied (CTR, BPH, and CA).

The volume fraction immunostained for ck18 is identical in the surrogate data compared to the corresponding real data in the three study groups, (Figure 2 b-d).

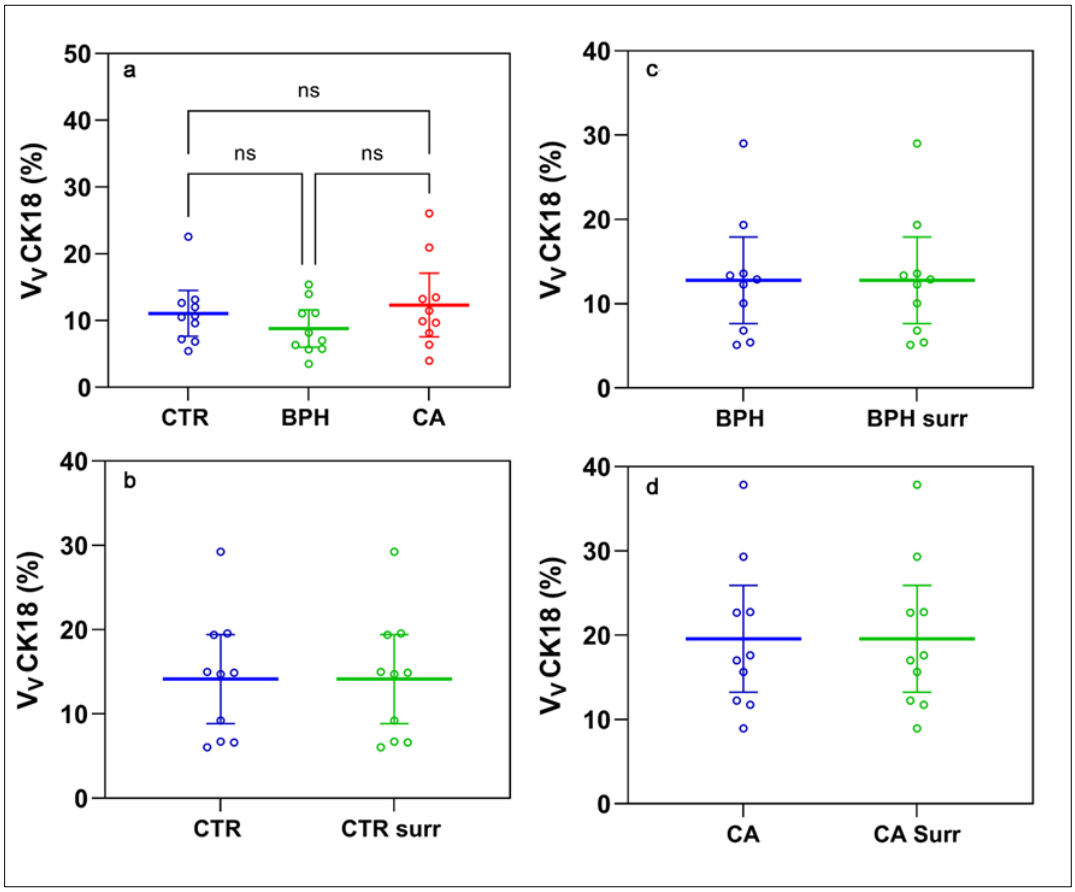

Figure 2 Scatter plots expressing both individual values (circles) and mean ± CI (95%) (horizontal lines) for volume fraction (V_VCK18) of prostate acini immunostained for cytokeratin 18. In (a) are shown CTR, BPH, and CA groups, ns indicates that there are no significant differences between groups; in (b) CTR and CTR surrogate data, (c) BPH and BPH surrogate data, and (d) CA and CA surrogate data

3.2 Multifractal Analysis

Multifractal spectra f(α) vs α: The multifractal spectrum of the ck18 positive acini of prostate shows a humped morphology with the branch of the graph of α values for Q ≤ 0 longer than that of the corresponding values for the range of values for Q ≥ 0, the values of α for the maximum values of f(α) (Q = 0) were 1.45, 1.42, and 1.64 for CTR, BPH, and CA groups, respectively. When the spectrum of the CTR data was compared with the spectra obtained for BPH and CA data, it was observed that both curves for BPH and CA moved to the right of the graph; this displacement was more important for the multifractal spectrum of CA cases in comparison with CTR cases. However, the curve shift of the BPH group was lesser compared to the curve for CTR cases (Figure 3 a,b). When the multifractal spectrum of the real data is compared with that generated by the surrogate data, it is observed that in the three study groups, the value of α corresponding to the maximum of f (α) is higher in the surrogate data concerning that of the real data, showing a relevant shift to the right of the surrogate f(α) curve, in CTR, BPH and CA groups (Figure 3 c-e).

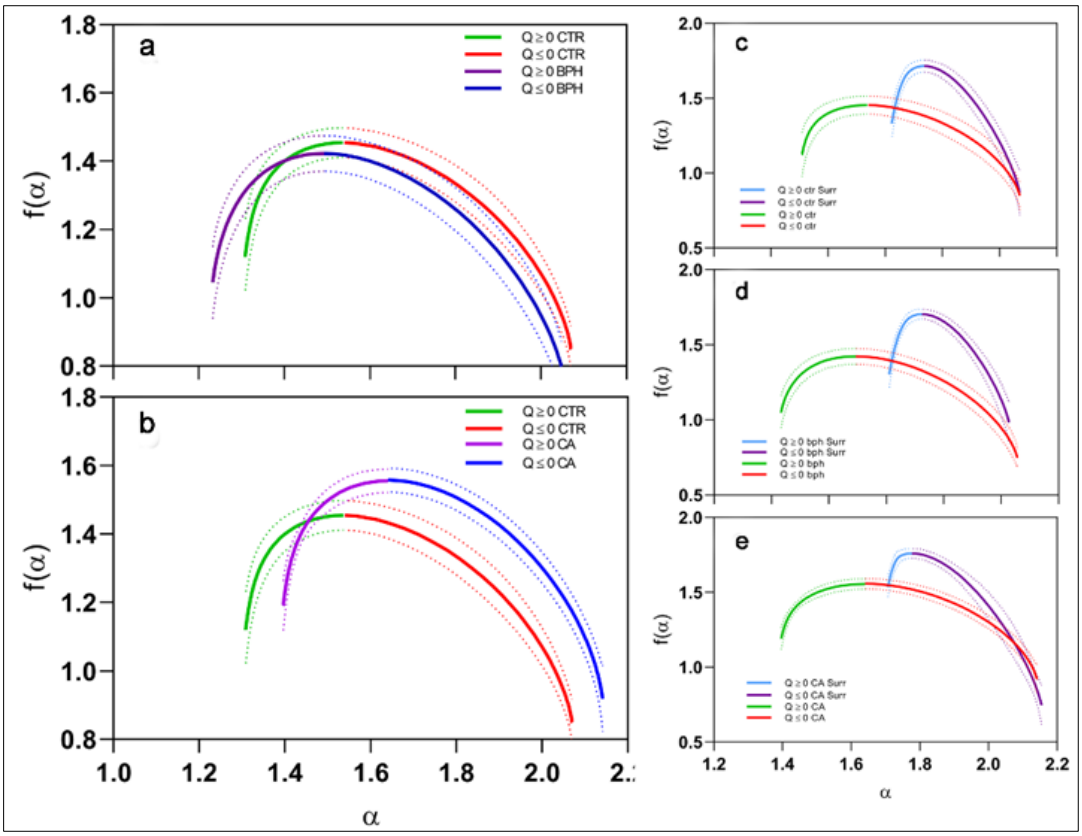

Figure 3 Multifractal spectra f(α) of prostate acini immunostained for ck18, in (a) are shown in CTR and BPH groups, in (b) CTR and CA groups. The branch of the curves for the range of Q ≥ 0 is indicated in green, and the branch for Q ≤ 0 in red in the CTR group; the branch of the curves for the range of Q ≥ 0 is indicated in violet and the branch for Q ≤ 0 in blue for both BPH (a) and CA (b) groups. Multifractal spectra f(α) of prostate acini immunostained for ck18 in real data (curves green-red) and surrogate data (curves blue-violet): In (c) are shown real and surrogate data for CTR, in (d) are shown real and surrogate data for BPH, and in (e) are shown real and surrogate data for CA. The values of the diverging exponent α are on the X axes, and the values of f(α) are on the Y axes. The dotted lines for each curve express the 95% confidence intervals (CI)

The Δα estimate from both real and surrogated data does not show significant differences between CTR, BPH, and CA groups (Figure 4 a,b). Nevertheless, a comparison of Δα for the real data with the surrogate data indicates that the Δα of the surrogate data of the three groups is significantly less than that of the respective real data (Figure 4 c-e).

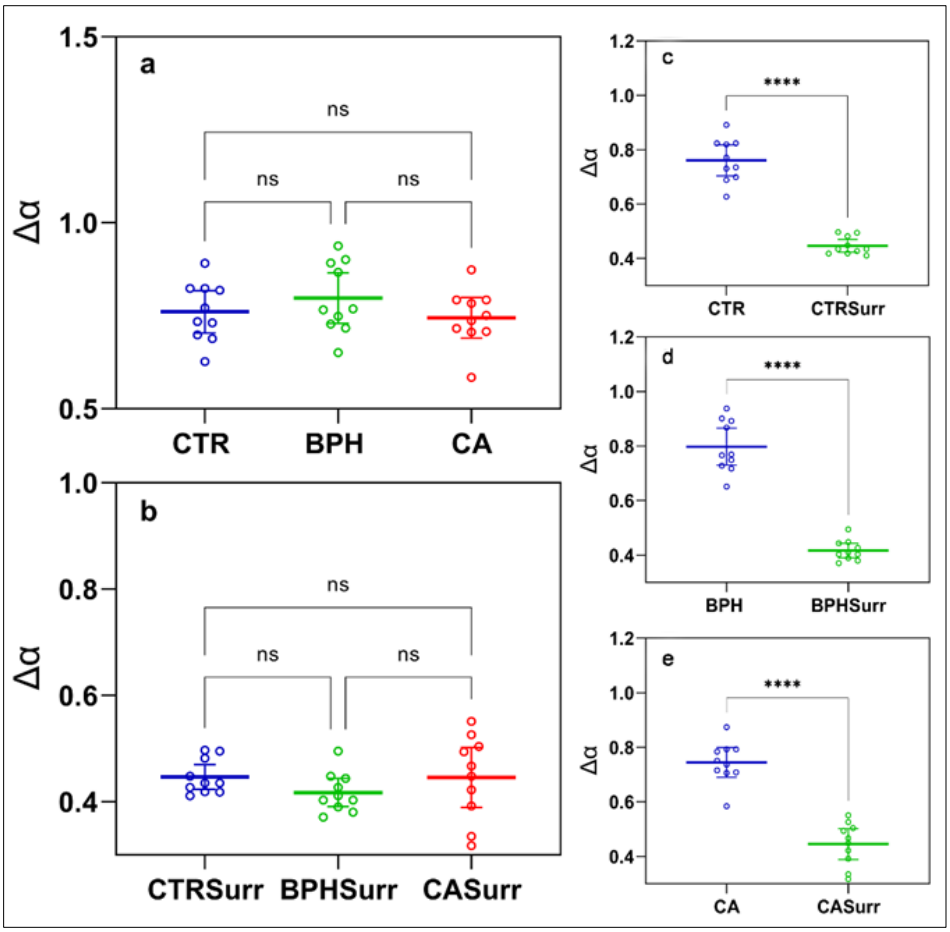

Figure 4 Scatter plots expressing both individual values (circles) and mean ± CI (95%) (horizontal lines) for the degree of multifractality (Δα) of prostate acini immunostained for cytokeratin 18. In (a) are shown the Δα values for real data of CTR, BPH, and CA, In (b) are shown the Δα values for surrogate data of CTR, BPH, and CA, ns indicates that there are no significant differences between groups; in (c) CTR and CTR surrogate data, (d) BPH and BPH surrogate data, and (e) CA and CA surrogate data. The asterisks indicate that there are significant differences between real and surrogate data ($p < 0.0001$)

The values of asymmetry (A) for all study groups in both the real and surrogate cases indicate that the f(α) spectra are always right-skewed ($A < 1$). For the real data the value of A in the CA group is higher than in the CTR and BPH groups, but that difference is significant only concerning CTR (Figure 5 a). For the surrogate data, A is significantly lower in CA about both CTR and BPH, however, the differences between CTR and BPH are not significant (Figure 5 b). When the A values of the real data are compared with the A values of their respective surrogates, the differences for CTR and BPH are not significant (Figure 5 c,d), however in the CA group, the A value for the surrogates is significantly lower than in the real data (Figure 5 e).

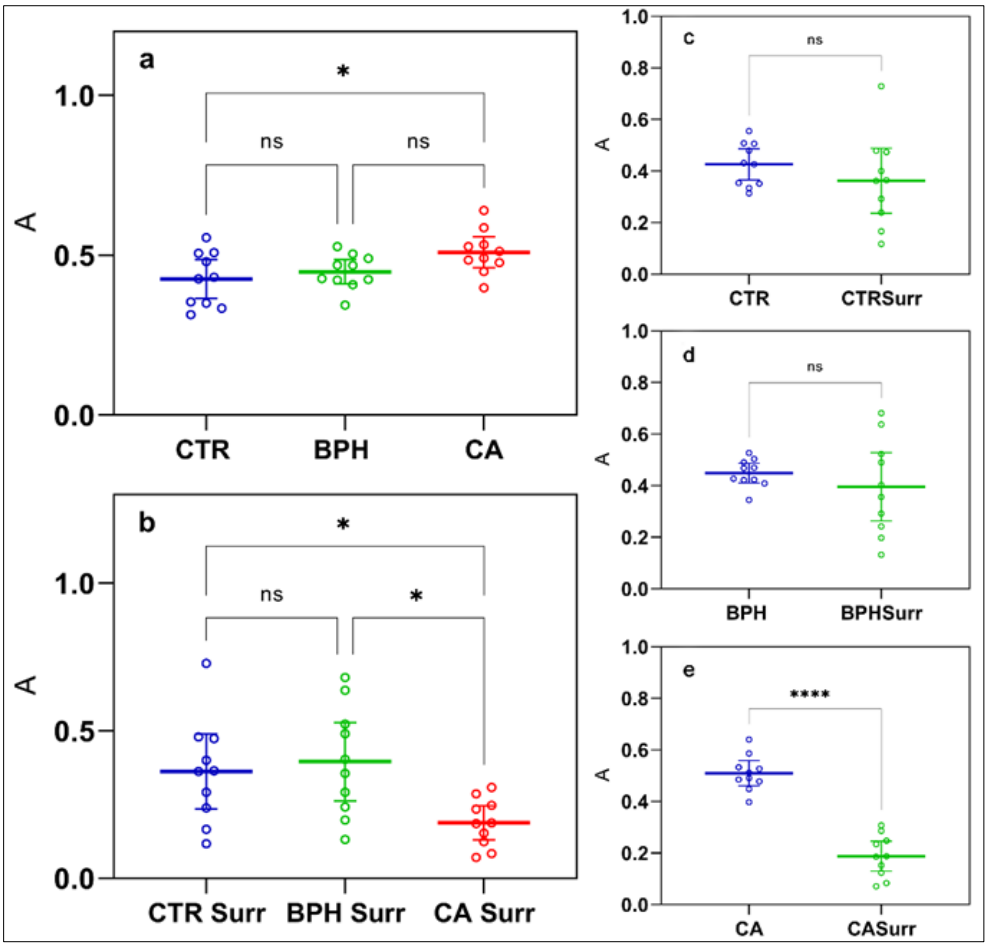

Figure 5 Scatter plots expressing both individual values (circles) and mean ± CI (95%) (horizontal lines) for asymmetry (A) of f(α) spectrum of prostate acini immunostained for cytokeratin 18. In (a) are shown the A values for real data of CTR, BPH, and CA, ns indicates that there are no significant differences between the groups affected, and the asterisk shows significant differences between CTR and CA groups ($p = 0.03$). In (b) are shown the A values for surrogate data of CTR, BPH, and CA, ns indicates that there are no significant differences between CTR surr and BPH surr groups, and asterisks show significant differences between affected groups ($p < 0.05$). In (c) CTR, and CTR surrogate data, (d) BPH, and BPH surrogate data, and (e) CA, and CA surrogate data. In (c) and (d) ns indicate that there are no significant differences between real and surrogate data, in (e) the asterisks indicate that there are significant differences between real and surrogate data ($p < 0.0001$)

Generalized dimension D_Q: In all the cases the graph of D_Q vs Q of the ck18 positive acini decreases and is sigmoidal around Q = 0. In the CTR and BPH groups, the corresponding curves do not show significant differences (Figure 6 a), while the curve of the cases of the CA group shows a slight but significant difference from the curve of the CTR group (Figure 6 b). The D_Q vs Q curves from the surrogate data in the three study groups shows significant differences when compared with the curves from the real data, so that the section of the curve corresponding to $Q > 0$ in the surrogate cases presents a greater linearity than in the same section for the real data (Figure 6 c-e).

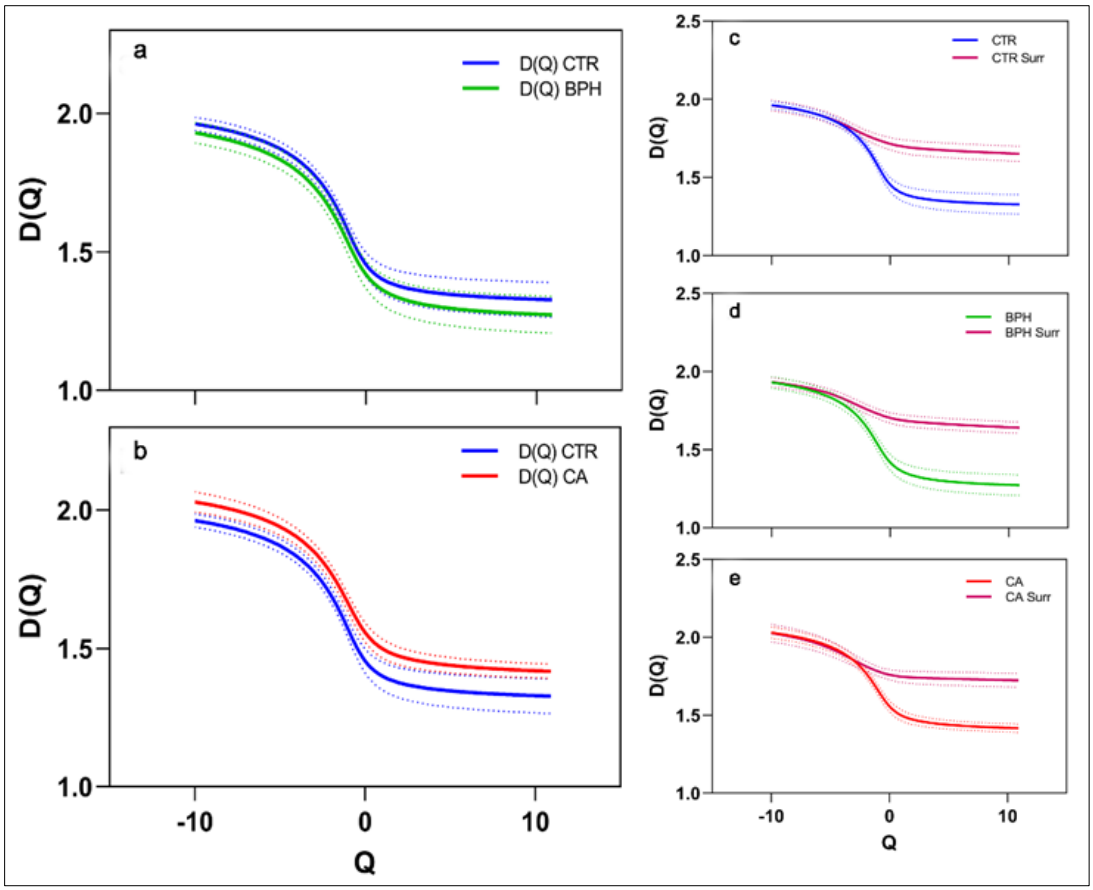

Figure 6 Graphs of the generalized dimension D(Q) as a function of Q. Q values are represented on the X axis, and D(Q) is on the Y axis. a: D(Q) obtained for prostate acini immunostained for ck18 in CTR and BPH groups, b: D(Q) obtained for prostate acini immunostained for ck18 in CTR and CA groups. Graphs of the generalized dimension D(Q) for real and surrogate data, c: D(Q) obtained for prostate acini immunostained for ck18 in CTR and CTR surr, d: D(Q) obtained for prostate acini immunostained for ck18 in BPH and BPH surr, e: D(Q) obtained for prostate acini immunostained for ck18 in CA and CA surr. The dotted lines for each curve express the 95% confidence intervals (CI)

The D_0 (capacity), D_1 (information), and D_2 (correlation) dimensions do not show significant differences when comparing the CTR group with the BPH group, while these values were significantly higher in the CA group compared to CTR (Figure 7 a,b). Dimensions D_0, D_1, and D_2 were significantly higher in the surrogate data compared to the real data for all three study groups (Figure 7 c-e).

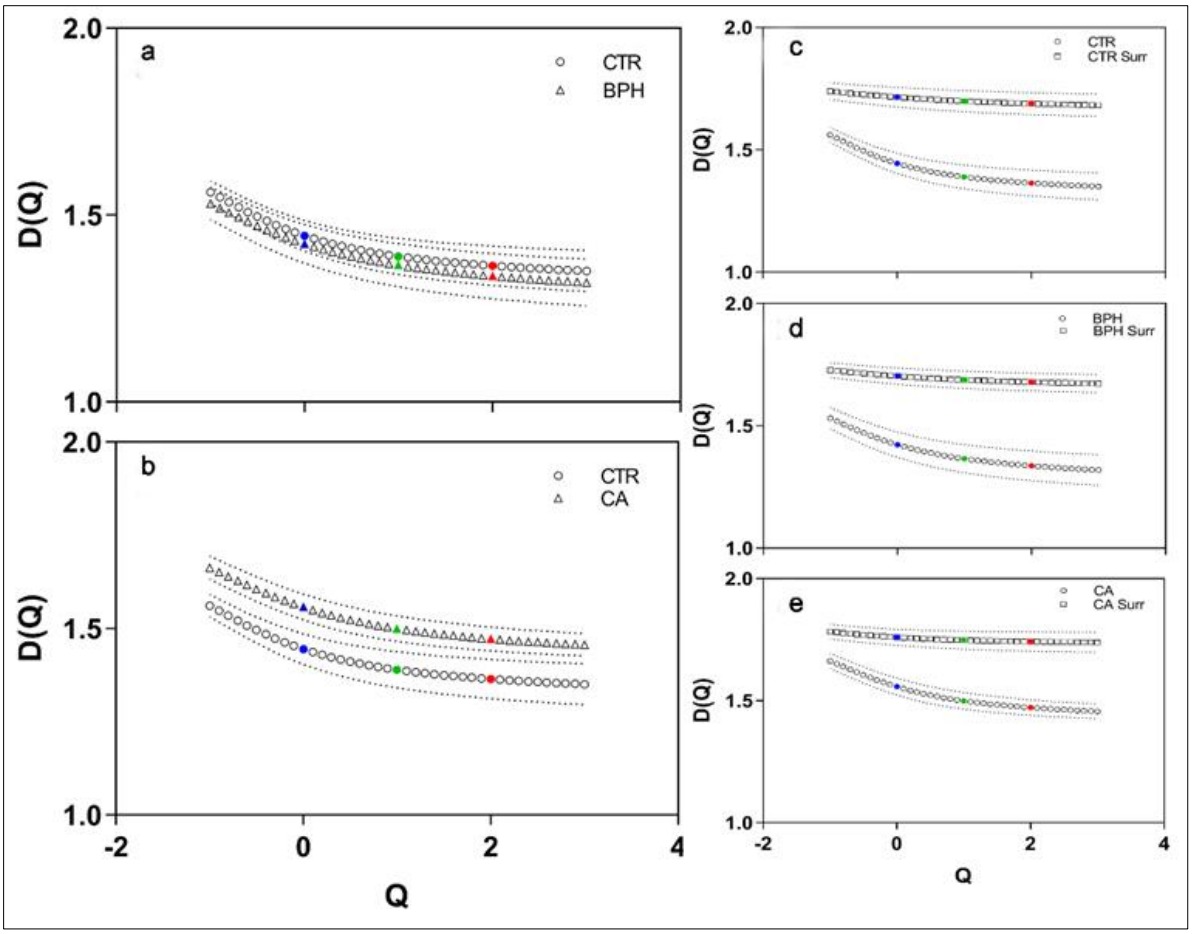

Figure 7 Section of the curve D(Q) between Q = 0 and Q = 2 to show the dimension of capacity Q_0 (blue), information Q_1 (green), and correlation Q_2 (red), a: curves for CTR and BPH,b: curves for CTR and CA. Section of the curves D(Q) for real and surrogate data between Q = 0 and Q = 2, c: curves for CTR and CTR surr, d: curves for BPH and BPH surr, e: curves for CA and CA surr. The dotted lines for each curve express the 95% confidence intervals (CI)

When the dimensions for Q = 0, Q = 1, and Q = 2 were compared to each other, the following results were observed: In the CTR group, D_2 is significantly lower than D_0, while there are no significant differences between D_0 and D_1 as well as between D_1 and D_2 (Figure 8 a). In the BPH group, no significant differences were detected between D_0, D_1, and D_2 (Figure 8 b). In the CA group, it is shown that D_0 is significantly greater than D_1 and D_2, while there are no significant differences between D_1 and D_2 (Figure 8 c). No significant differences were observed between D_0, D_1, and D_2 for the surrogate data from the three study groups (Figure 8 d-f).

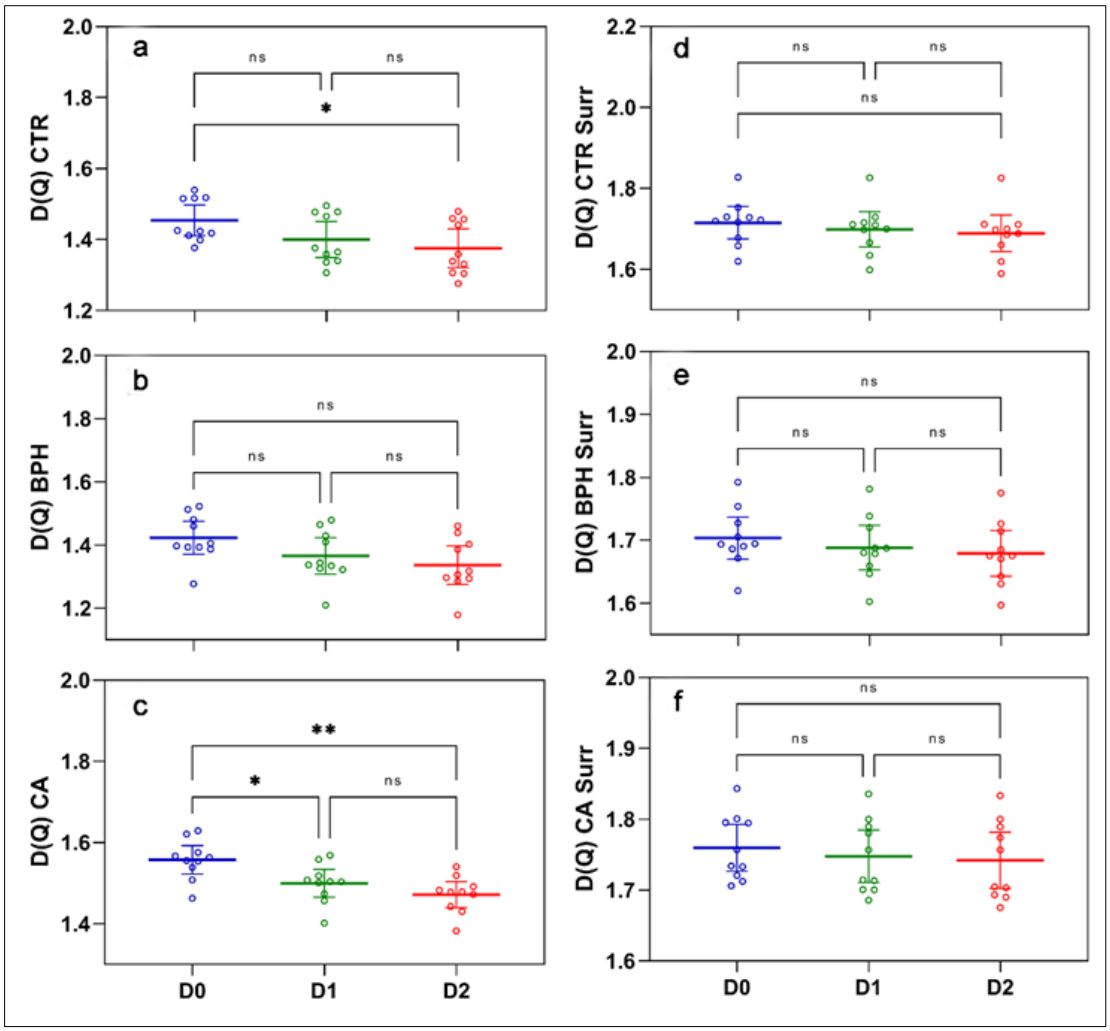

Figure 8 Scatter plot expressing both individual values (circles) and mean ± CI (95%) (horizontal lines) for comparison of the dimension of capacity D_0 (blue), information D_1 (green), and correlation D_2 (red), of prostate acini immunostained for of cytokeratin 18 in CTR (a), BPH (b), and CA (c) groups, and surrogate data, CTR surr (d), BPH surr (e), and CA surr (f) groups, ns indicates that there is not significant differences between values affected, individual asterisk indicates that are significant differences (p = 0.04) between values affected, and two asterisks indicate that are significant differences (p = 0.001) between values affected

3.3 Local connected fractal dimension analysis

The local connected fractal dimension (LCFD) of the ck18 positive acini of the prostate shows no significant differences between the CTR, BPH, and CA groups, both for the real data and for the surrogate data (Figure 9 a,b). The LCFD of the surrogate data is in all cases significantly lower compared to the real data (Figure 9 c-e).

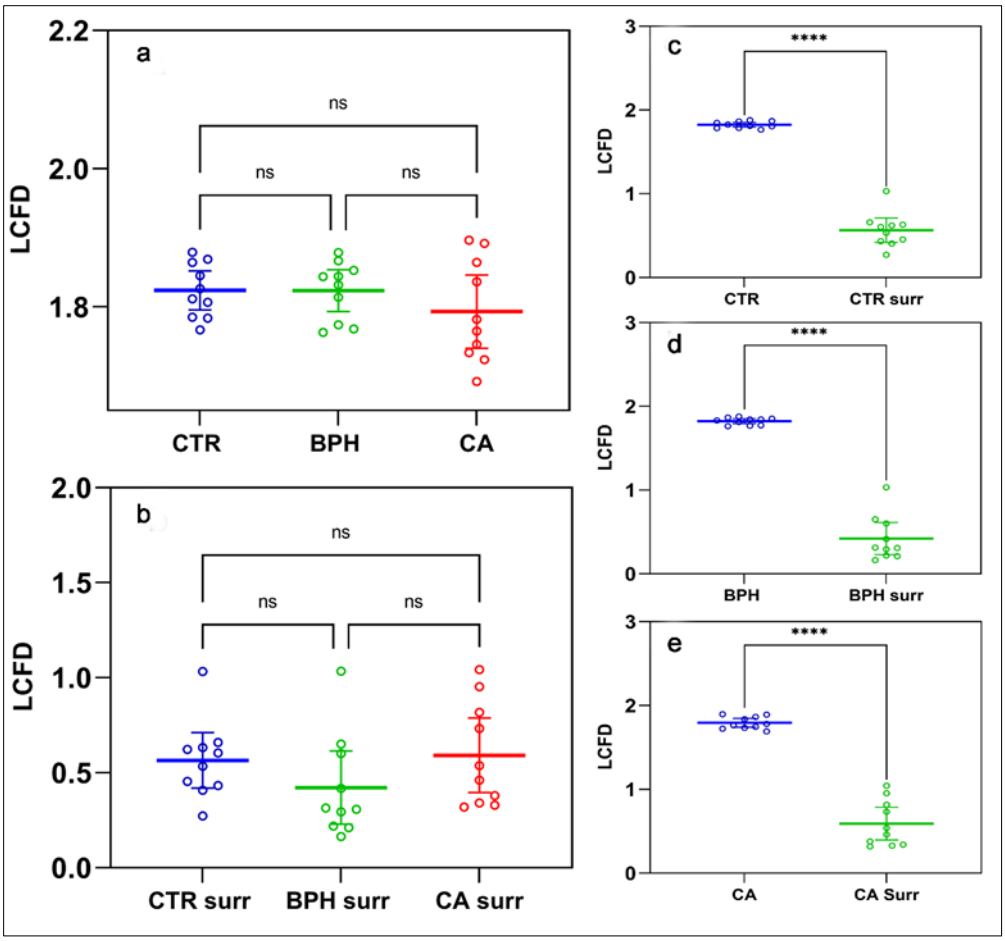

Figure 9 Scatter plots expressing both individual values (circles) and mean ± CI (95%) (horizontal lines) for local connected fractal dimension (LCFD) of prostate acini immunostained for cytokeratin 18. In (a) are shown the LCFD values for real data of CTR, BPH, and CA, in (b) are shown the LCFD values for surrogate data of CTR, BPH, and CA, in (c) CTR and CTR surrogate data, (d) BPH and BPH surrogate data, and (e) CA and CA surrogate data. The asterisks indicate that there are significant differences between real and surrogate data ($p < 0.0001$), and ns indicates that there are no significant differences between groups, in both real and surrogate data

The frequency histogram of the LCFD distribution was similar when comparing the CTR and BPH groups, with an almost complete overlap of the two frequency curves (Figure 10 a), while the histogram of the CA group compared to that of the CTR group, indicated that in the LCFD range between 1.78 and 1.88 the frequencies of occurrence were significantly lower for the CA group (Figure 10 b). The frequency histogram of the LCFD distribution of the surrogate data was similar in all groups, with decreasing frequency peaks being observed in the LCFD range from 0.0 to 0.83 (Figure 10 c-e).

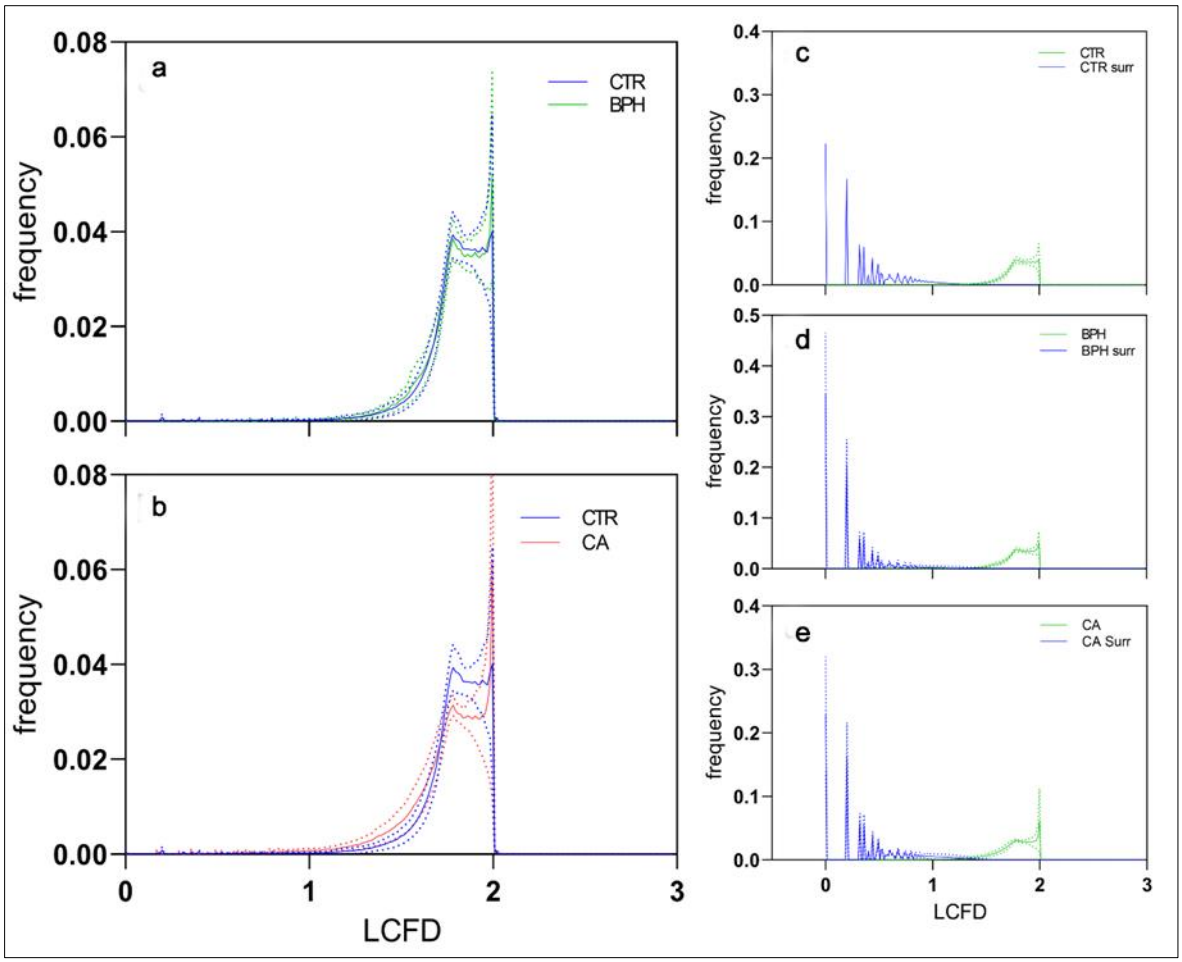

Figure 10 Frequency histograms of LCFD, in (a) are shown the histograms for CTR and BPH, in (b) are shown the histograms for CTR and CA, in (c) are shown the histograms for CTR and CTR surrogate data, in (d) are shown the histograms for BPH and BPH surrogate data, in (e) are shown the histograms for CA and CA surrogate data. The dotted lines for each curve express the 95% confidence intervals (CI)

3.4 Lacunarity analysis

The lacunarity (Λ) of prostatic acini immunostained for ck18 is significantly greater in the CA group compared to the CTR and the BPH groups, while no significant differences were observed between the CTR and BPH groups (Figure 11 a). When Λ of the surrogate data was analyzed, no significant differences were detected between the three study groups (Figure 11 b). The lacunarity of the surrogate data is in all cases significantly lower compared to the real data (Figure 11 c-e).

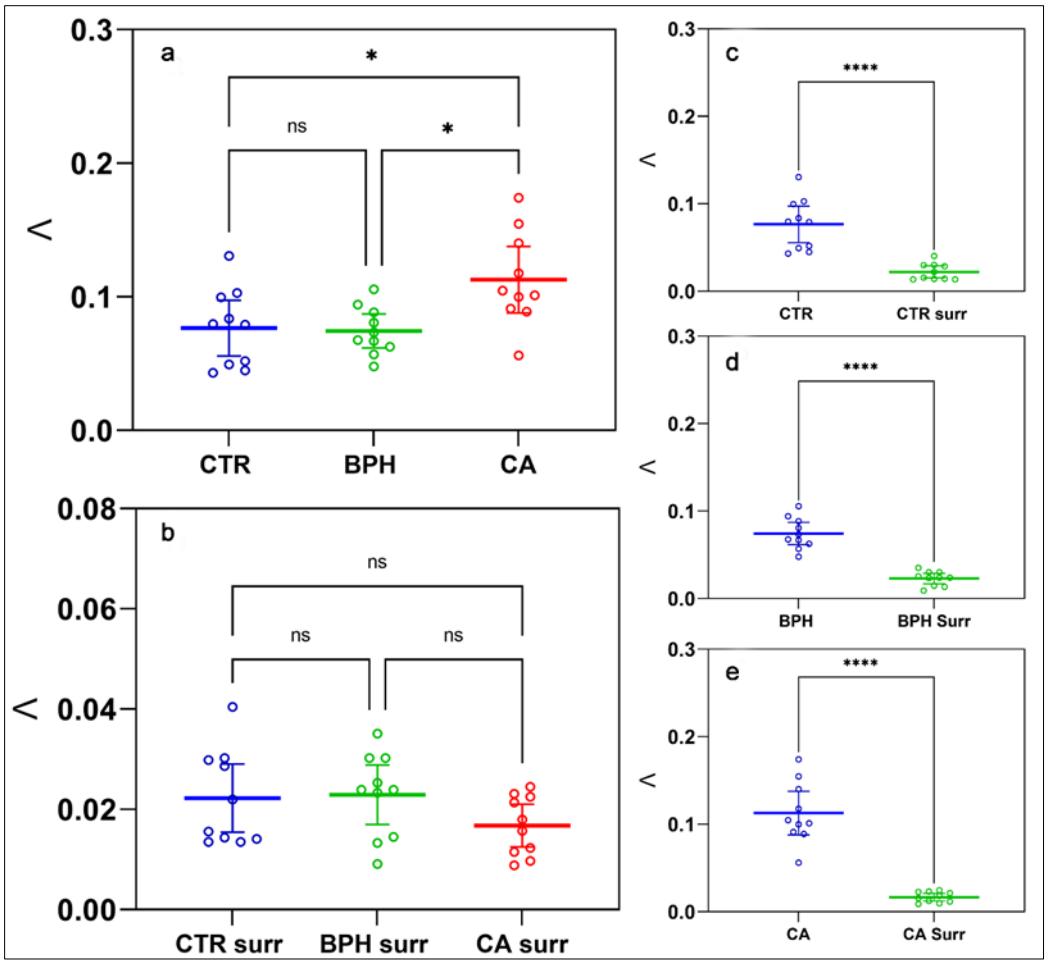

Figure 11 Scatter plots expressing both individual values (circles) and mean ± CI (95%) (horizontal lines) for lacunarity (Λ) of prostate acini immunostained for cytokeratin 18. In (a) are shown the Λ values for real data of CTR, BPH, and CA, and in (b) are shown the Λ values for surrogate data of CTR, BPH, and CA. The asterisk indicates that there are significant differences between groups affected ($p = 0.0203$), and ns indicates that there are no significant differences between groups affected. In (c) are shown CTR and CTR surrogate data, (d) BPH and BPH surrogate data, and (e) CA and CA surrogate data. The asterisks indicate that there are significant differences between real and surrogate data ($p < 0.0001$)

When Λ is analyzed as a function of the scale ε, a parabola-shaped curve is obtained in both CTR, BPH, and CA. When comparing the curve of the CTR cases with that of the BPH cases, an almost complete overlap of both graphs was observed (Figure 12 a), if the CTR curve is compared with that of the CA cases, a slight shift of the CA graph to the left is shown (Figure 12 b). In the three study groups it is observed that the plot of the Λ vs ε of the surrogate data has a very different morphology from the curves produced by the real data, the parabolic shape is lost, and a linear section is observed in the ε range between -4 and -1 (on a logarithmic scale) (Figure 12 c-e).

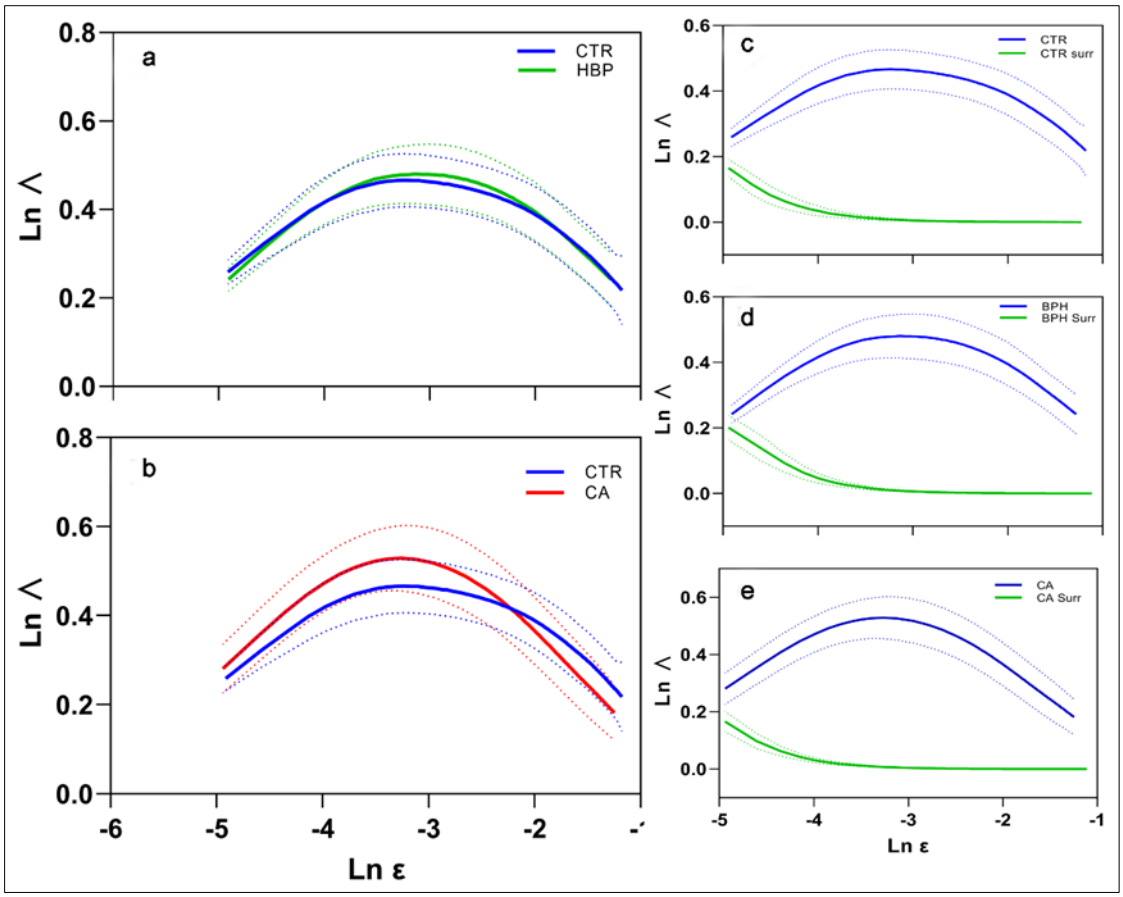

Figure 12 Graphs representing Λ of the acini immunostained for ck 18 as a function of ε (on a logarithmic scale), in (a) are shown the curves for CTR and BPH, in (b) are shown the curves for CTR and CA, in (c) are shown the curves for CTR and CTR surrogate data, in (d) are shown the curves for BPH and BPH surrogate data, and in (e) are shown the curves for CA and CA surrogate data. The dotted lines for each curve express the 95% confidence intervals (CI)

3.5 Principal components analysis

With the six variables introduced in the analysis, 6 principal components were obtained, of which, PC1 and PC2 explained more than 70% of the variance, both for the analysis with the real data and for the surrogate data (Figure 13 a,b). Analyzing the loading plot for the real data, (Figure 13 c) we can see that variables D_0, D_1, and Λ are strongly correlated (values close to 1) with PC1, while they are only somewhat correlated with PC2, variable A is also weakly correlated with PC1, Conversely, variable LCFD correlate strongly with PC2, and there is also observed a negative correlation of Δα with PC1, but these two variables are only somewhat negatively correlated with PC1. As shown on this graph, variables D_0, and D_2, are clustered closely together, indicating that these 2 variables are positively correlated. In comparison, the vectors for variables LCFD and A form a nearly 180° angle, indicating that these variables are negatively correlated. Finally, the vector for variable LCFD forms a nearly right angle with vectors for D_0, D_2, and Δα, suggesting that LCFD is likely uncorrelated with those other three vectors. The loading plot for the surrogate data (Figure 13 d) shows important changes about the real data: Variables D_0, and D_2 are strongly correlated (values close to -1) with PC1, and PC2. Meanwhile, variable Λ correlates strongly with PC2 but is only somewhat correlated with PC1. Furthermore, D_0 and D_2 on the one hand and Δα, Λ, and A on the other appear closely clustered together, indicating that each group of variables is positively correlated. In comparison, the vectors for D_0, and D_2 form a nearly 180° angle with the vector for LCFD, indicating that these two variables are negatively correlated with LCFD.

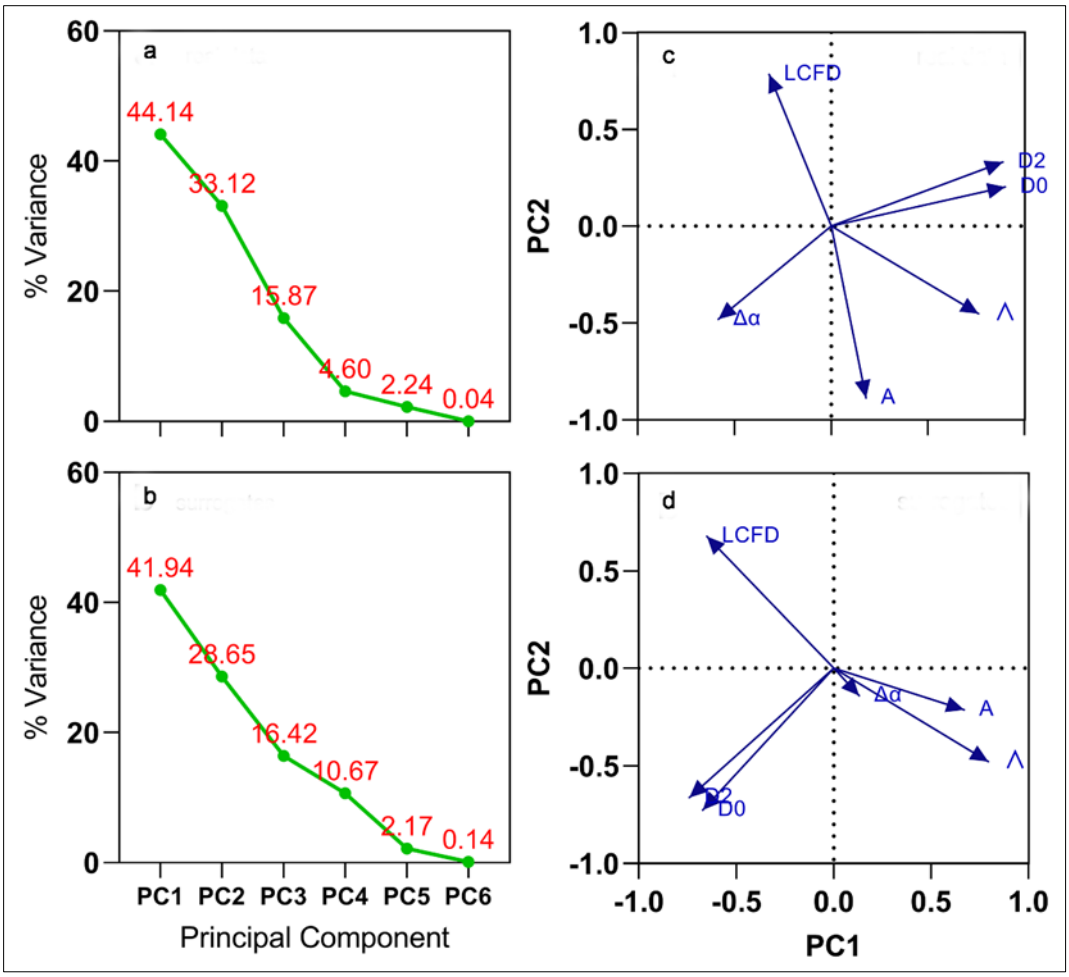

Figure 13 In (a) and (b) are shown graphs expressing the percentage of variance explained by each of the six principal components (PC). The numbers in red indicate the % of variance explained by each PC, for the real data (a) and the surrogate data (b). In (c) and (d) are shown graphs expressing the loading plot of variables correlated with principal component 1 (PC1) in X axis, and principal component 2 (PC2) in Y axis. The variables are Local connected fractal dimension (LCFD), capacity dimension (D_0), correlation dimension (D_2), lacunarity (Λ), f(α) spectrum asymmetry (A), and the degree of multifractality (Δα). In (a) is shown the loading plot for real data, and in (b) for the surrogate data

The PC-scores indicate that the PC1 vs PC2 graph displays the distribution of cases of the CA group in the region delimited by PC1 with values from 0 to 4 and by PC2 with values from -4 to 4, while the cases of CTR and BPH groups are predominantly distributed in the symmetric region: PC1 in a range of values from 0 to -4 and PC2 in a range from -4 to 4 (Figure 14 a). The PC-score of PC1 vs PC2 for the surrogated data shows a more homogeneous distribution of cases without a defined data clustering (Figure 14 b).

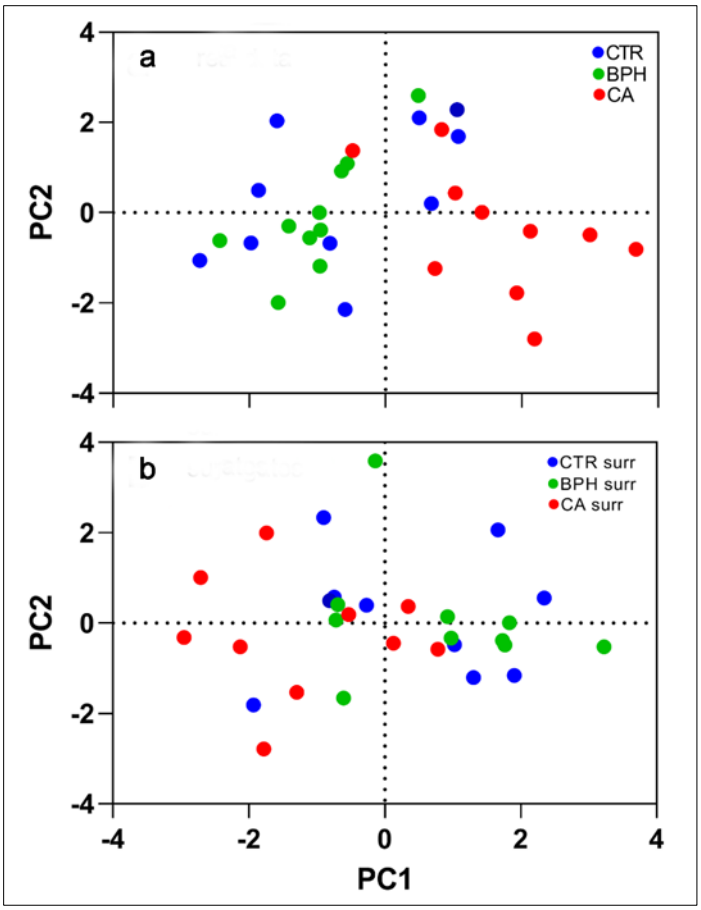

Figure 14 Graphs expressing the scores for PC1 and PC2 from CTR (blue), BPH (green), and CA (red) cases in (a) real data, and (b) surrogate data

The contingency analysis shows that the predominant distribution of the CA group in a region of the PC1 vs PC2 graph, delimited by the range of PC1 between 0 and -4 and by the range of PC2 between -4 and 4 in comparison to the distribution of the CTR and BPH groups, is significant for the Chi^2 test (Figure 15 a). For the surrogate data, the distribution of data from CTR, BPH, and CA is homogeneous and does not show significant clustering in any region of the PC1 vs PC2 map (Figure 15 b).

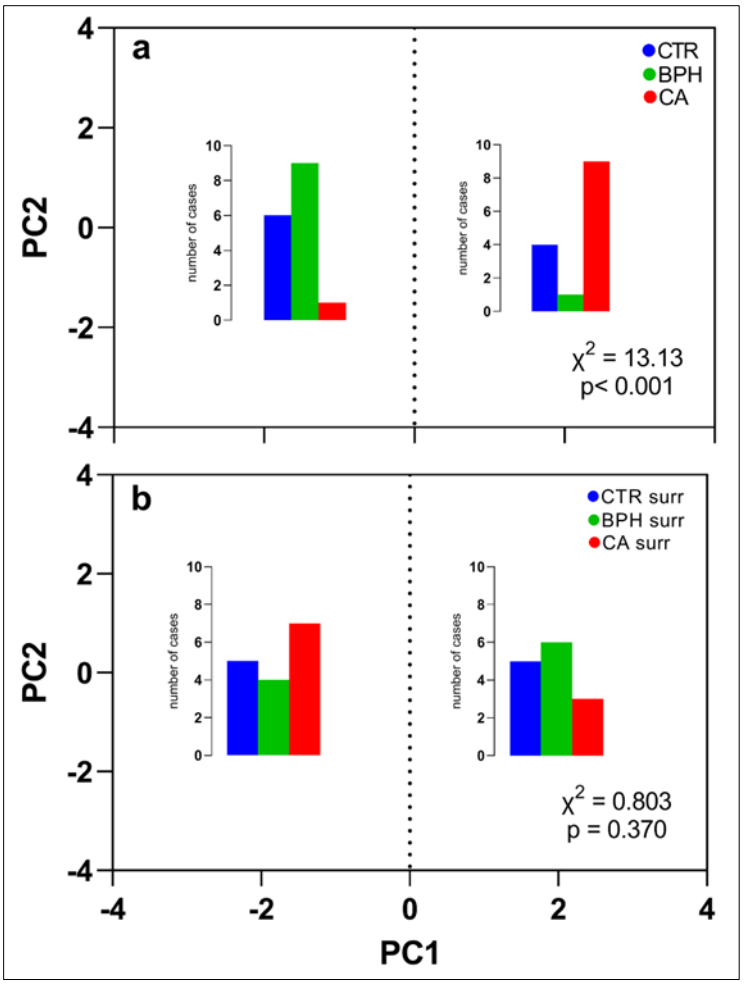

Figure 15 Graphs expressing the contingency analysis results that show the predominant distribution of the CA group (red) in a region of the PC1 vs PC2 graph, delimited by the range of PC1 between 0 and -4 and by the range of PC2 between -4 and 4 in comparison to the distribution of the CTR (blue) and BPH (green) groups. According to the Chi2 test, the heterogeneity of distribution is significant for real data (a), and not significant for surrogate data (b)

4 Discussion

As has already been shown in other studies (*Santamaría L, et al. 2016; Santamaría L, et al. 2017*), no significant differences were observed in the acinar volume fraction immunostained for ck18 in controls (CTR) and in both benign (BPH) and malignant (CA) prostate pathology; the differences in V_V ck18 are more related with the heterogeneity of immunostaining and its possible fractal structure. As expected, the V_V ck18 of the real data is identical to that measured in the surrogate data, since the difference between these is only due to the shuffling of the immunostained pixels (*Spasic S, et al. 2011*) without an increase or decrease in those pixels compared to real cases. This study indicates that the distribution of acini immunoreactive for ck18 in normal and pathological prostate (benign hyperplasia and adenocarcinoma) shows a multifractal structure, like those observed in other biological structures as diverse as the cholinergic innervation of the testicular albuginea of the rat (*Santamaria L and Ingelmo I 2023*), or the immunoexpression of several lens proteins from mice with folic acid dietary deficiency (*Sijilmassi Q, et al. 2020*). Therefore, it confirms what was stated by other authors (*Atupelage C, et al. 2012*) about the importance of the multifractal feature as a descriptor in histopathology, and emphasizes the interest in the multifractal methods applied to cellular morphology (*Smith TG, Jr., et al. 1996*). Interesting differences are observed in the multifractality of prostate cancer compared to normal prostate and BPH: The f(α) spectrum shows a very similar structure in CTR and BPH, while in CA the maximum value of f(α) (Q = 0) is significantly higher, although the degree of multifractality estimated by Δα is similar in all groups. Also, the estimation of the asymmetry (A) indicates that in all cases, values of A < 1 predominate, that is, f(α) is right-skewed, which suggests that low fractal exponents and small fluctuations dominate the measure in all groups (*Hu MG, et al. 2009*). Although the mean value of A (0.51) in the CA group is indicative of right skewness, it is significantly higher than in CTR and BPH, therefore the degree of asymmetry in cases of a malignant tumor is lower than

in normal prostate and in the hyperplastic prostate. This study demonstrates that the spatial arrangement of ck 18 immunostained acini in prostate adenocarcinoma can be quantified and separated from the normal and benignant acini by the properties of their f(α)-spectra, as described in structures not related to biological elements, i.e. soil sciences (*Posadas AND, et al. 2003*). When the changes in the generalized dimension D_Q as a function of Q are studied, parallelism is observed with what was described for the spectrum f(α): similarity of results in the CTR and BPH cases and difference of both with the CA group. The relationships between capacity dimension (D_0), information dimension (D_1), and correlation dimension (D_2) are preserved in the three groups ($D_0 \geq D_1 \geq D_2$) (*Santamaria L and Ingelmo I 2023*) but the decrease in the values from D_0 to D_2 is more manifest in CA, which may suggest greater multifractality in that group (*Gammel BM 1994*). The random distribution of pixels immunostained for ck 18 in the surrogate data does not suppress multifractality, but greatly modifies it compared to the real data in the three study groups: The f(α) graphs of the surrogate data are more humped than in the real data, but Δα indicates a lower degree of multifractality in the surrogate data, while the skewness is similar compared to the real data. Furthermore, in the surrogate data, there are no significant differences between D_0, D_1, and D_2, which indicates that the surrogate data acquire a profile close to mono-fractality (*Gammel BM 1994*). Although the average LCFD values are similar in the three groups, the frequency distribution of LCFD values is similar in CTR and BPH, but differs in the CA group about the other two, with the population of LCFD values being smaller in a small range, this may suggest a greater disconnection between the pixels immunostained for ck18 in the CA group that is a greater local variation in complexity (*Landini G, et al. 1995; Manera M, et al. 2013*), which could be related to greater heterogeneity of the tumor acini (*Santamaria L, et al. 2018*). The random distribution of immunostained pixels in the surrogate data can be related to the significant decrease in LCFD values in that data, together with a heterogeneous distribution of LCFD frequency histogram values. No significant differences in Λ were observed at a global level between CTR and BPH, although in other studies (*Santamaría L, et al. 2017*) local differences in lacunarity were detected between these study groups, however, the classification power of the Λ parameter poorly discriminated between normal prostate and hyperplastic prostate (*Santamaría L, et al. 2017*). The significant increase in lacunarity of ck18-immunostained acini in cancer compared to BPH and normal prostate supports a wider range of sizes of structures within an image (*Dougherty G and Henebry GM 2002*), i.e. the heterogeneity of tumor acini compared to normal acini (*Santamaria L, et al. 2018*). In turn, it is observed that the random distribution of ck18 immunostaining pixels in the surrogate data implies a homogenization of tissue texture and a decrease in lacunarity that affects the three groups studied (*Cordeiro MS, et al. 2016*). In all cases of real data (CTR, BPH, and CA) the graph of Λ as a function of scale ε presents a parabolic morphology, this agrees with the analysis of the lacunarity of the texture of structures grouped in clusters (the acini) separated by gaps of variable magnitude (*Plotnick RE, et al. 1996*); however, the graph of the lacunarity of the surrogate data is compatible with a homogeneous and regularly spaced distribution of elements, as occurs with the immunostained pixels of the surrogate data (*Plotnick RE, et al. 1996*). The principal component analysis shows interesting interrelations between the variables studied: the local character dimension (LCFD) does not seem to correlate significantly with the introduced D_Q (D_0, D_2), nor with the degree of multifractality Δα, however, it has a negative correlation with the asymmetry of the spectrum f(α) and to a lesser extent with Λ. In any case, a complementarity between fractality and lacunarity can be observed, as has been shown in other studies (*Borys P, et al. 2008*). The plot of the first and second components shows that PCA helps to improve the separation of the two classes of samples (*Cordeiro MS, et al. 2016*). On the one hand, the malignant tumor group (CA) and on the other, the normal (CTR) and benign hyperplastic (BPH) groups, which do not show discrimination between them. When the real data are replaced by the surrogated data in the PCA, this separation between the three study groups disappears.

5 Conclusion

The distribution of ck18-immunostained acini shows a multifractal structure in both normal and pathological prostate. However, the degree of multifractality in prostatic adenocarcinoma is significantly higher than in normal prostate and BPH. It is also observed that the heterogeneity of the acinar structure of the cancer is greater than in controls and BPH, as indicated by lacunarity and to a lesser extent by LCFD. The fractal and lacunarity variables introduced in the Principal Components Analysis discriminate the prostatic adenocarcinoma group from the normal prostate and BPH groups. The surrogate model destroys the structural relationships that the real data show, and this results in a decrease in multifractality and lacunarity. It also eliminates the discriminating power of the variables introduced in the PCA.

Compliance with ethical standards

Acknowledgments

The authors would like to thank for technical support to Carmen Sánchez (Department of Anatomy, Histology, and Neuroscience, UAM).

Disclosure of conflict of interest

All author declared that they have no conflict of interest.

Statement of informed consent

Informed consent for the use of surgical specimens or biopsies, issued by the Bioethics Committee of the Hospital Universitario de La Princesa (Madrid, Spain) was accomplished to obtain the prostate tissue either when the multi-organic extraction for transplant (CTR) or at the surgery (BPH and CA).

References

[1] Arriazu R, Pozuelo JM, Martin R, Rodriguez R, Santamaria L. (2005). Quantitative and immunohistochemical evaluation of PCNA, androgen receptors, apoptosis, and Glutathione-S-Transferase P1 on preneoplastic changes induced by cadmium and zinc chloride in the rat ventral prostate. Prostate. 63(4):347-57. https://doi.org/10.1002/pros.20192

[2] Atupelage C, Nagahashi H, Yamaguchi M, Sakamoto M, Hashiguchi A. (2012). Multifractal feature descriptor for histopathology. Analytical Cellular Pathology. 35:123-6. https://doi.org/10.3233/ACP-2011-0045

[3] Baddeley A and Vedel Jensen E. (2005). Uniform and Isotropic Uniform Designs. En: Baddeley A and Vedel Jensen E, editors. Stereology for Statisticians. Boca Raton: Chapman and Hall. pp:155-73.

[4] Barry MJ. (1990). Epidemiology and natural history of benign prostatic hyperplasia. Urol Clin North Am. 17(3):495-507.

[5] Bartsch G. (1977). Stereology, a new quantitative morphological approach to study prostatic function and disease. Eur Urol. 3(2):85-95. https://doi.org/10.1159/000472066

[6] Barwick K and Mardi A. (1983). An immunohistochemical study of the myoepithelial cell in prostate hyperplasia and neoplasia. Lab Invest. 48:7A.

[7] Berry SJ, Coffey DS, Walsh PC, Ewing LL. (1984). The development of human benign prostatic hyperplasia with age. J Urol. 132(3):474-9. https://doi.org/10.1016/s0022-5347(17)49698-4

[8] Birkhoff JD. (1983). Natural History of Benign Prostatic Hypertrophy. In: Hinman F, editor. Benign Prostatic Hypertrophy. New York: Springer Verlag. pp:5-14.

[9] Borys P, Krasowska M, Grzywna ZJ, Djamgoz MB, Mycielska ME. (2008). Lacunarity as a novel measure of cancer cells behavior. Biosystems. 94(3):276-81. https://doi.org/10.1016/j.biosystems.2008.05.036

[10] Brawer MK, Peehl DM, Stamey TA, Bostwick DG. (1985). Keratin immunoreactivity in the benign and neoplastic human prostate. Cancer Res. 45(8):3663-7.

[11] Burgos Rodríguez R and Chicharro Molero JA. (1993). Hiperplasia Benigna de Próstata. En: Jiménez Cruz JF and Rioja Sanz LA, editors. Tratado de urología. Barcelona: J.R.Prous. pp:1035-50.

[12] Cordeiro MS, Backes AR, Junior AF, Goncalves EH, de Oliveira JX. (2016). Fibrous Dysplasia Characterization Using Lacunarity Analysis. J Digit Imaging. 29(1):134-40. https://doi.org/10.1007/s10278-015-9815-3

[13] Dougherty G and Henebry GM. (2002). Lacunarity analysis of spatial pattern in CT images of vertebral trabecular bone for assessing osteoporosis. Med Eng Phys. 24(2):129-38. https://doi.org/10.1016/s1350-4533(01)00106-0

[14] Festuccia C, Angelucci A, Gravina GL, Muzi P, Miano R, Vicentini C, et al. (2005). Epithelial and prostatic marker expression in short-term primary cultures of human prostate tissue samples. Int J Oncol. 26(5):1353-62.

[15] Fitzpatrick JM. (2006). The natural history of benign prostatic hyperplasia. BJU Int. 97:3-6; discussion 21-2. https://doi.org/10.1111/j.1464-410X.2006.06097.x

[16] Franke WW, Appelhans B, Schmid E, Freudenstein C, Osborn M, Weber K. (1979). Identification and characterization of epithelial cells in mammalian tissues by immunofluorescence microscopy using antibodies to prekeratin. Differentiation. 15(1):7-25. https://doi.org/10.1111/j.1432-0436.1979.tb01030.x

[17] Gammel BM. (1994). Kritisches Verhalten und Niederfrequenz-Anomalien beim Quanten-Hall-Effekt. Doktors der Naturwissenschaften (Dr. rer. nat.). München Technischen Universität München, Fakultät für Physik. 100pp

[18] Goldberger AL, Amaral LA, Hausdorff JM, Ivanov P, Peng CK, Stanley HE. (2002). Fractal dynamics in physiology: alterations with disease and aging. Proc Natl Acad Sci U S A. 99(Suppl 1):2466-72. https://doi.org/10.1073/pnas.012579499

[19] Horn JL. (1965). A Rationale and Test for the Number of Factors in Factor Analysis. Psychometrika. 30:179-85. https://doi.org/10.1007/BF02289447

[20] Howard CV and Reed MG. (1998). Unbiased Stereology: Three-Dimensional Measurement in Microscopy. Oxford: Garland Science/BIOS Scientific Publishers.

[21] Hu MG, Wang JF, Ge Y. (2009). Super-resolution reconstruction of remote sensing images using multifractal analysis. Sensors (Basel). 9(11):8669-83. https://doi.org/10.3390/s91108669

[22] Humphrey PA. (2004). Gleason grading and prognostic factors in carcinoma of the prostate. Mod Pathol. 17(3):292-306. https://doi.org/10.1038/modpathol.3800054

[23] Iczkowski KA, Torkko KC, Kotnis GR, Wilson RS, Huang W, Wheeler TM, et al. (2011). Pseudolumen size and perimeter in prostate cancer: correlation with patient outcome. Prostate Cancer. 2011:693853. https://doi.org/10.1155/2011/693853

[24] Isaacs JT. (1994). Etiology of benign prostatic hyperplasia. Eur Urol. 25(Suppl 1):6-9. https://doi.org/10.1159/000475324

[25] Ivanov PC, Amaral LA, Goldberger AL, Havlin S, Rosenblum MG, Struzik ZR, et al. (1999). Multifractality in human heartbeat dynamics. Nature. 399(6735):461-5. https://doi.org/10.1038/20924

[26] Karperien A, Jelinek HF, Leandro JJ, Soares JV, Cesar RM, Jr., Luckie A. (2008). Automated detection of proliferative retinopathy in clinical practice. Clin Ophthalmol. 2(1):109-22. https://doi.org/10.2147/opth.s1579

[27] Kirby RS. (1992). The clinical assessment of benign prostatic hyperplasia. Cancer. 70(Suppl 1):284-90. https://doi.org/10.1002/1097-0142(19920701)70:1+<284::aid-cncr2820701316>3.0.co;2-#

[28] Landini G, Murray PI, Misson GP. (1995). Local connected fractal dimensions and lacunarity analyses of 60 degrees fluorescein angiograms. Invest Ophthalmol Vis Sci. 36(13):2749-55.

[29] Landini G and Rippin JW. (1993). Fractal dimensions of the epithelial-connective tissue interfaces in premalignant and malignant epithelial lesions of the floor of the mouth. Anal Quant Cytol Histol. 15(2):144-9.

[30] Landini G and Rippin JW. (1996). How important is tumour shape? Quantification of the epithelial-connective tissue interface in oral lesions using local connected fractal dimension analysis. J Pathol. 179(2):210-7. https://doi.org/10.1002/(SICI)1096-9896(199606)179:2<210::AID-PATH560>3.0.CO;2-T

[31] Losa GA and Nonnenmacher TF. (1996). Self-similarity and fractal irregularity in pathologic tissues. Mod Pathol. 9(3):174-82.

[32] Mandelbrot BB. (1974). Intermittent turbulence in self-similar cascades: divergence of high moments and dimension of the carrier Journal of Fluid Mechanics. 62(2):331-58. https://doi.org/10.1017/S0022112074000711

[33] Manera M, Giari L, De Pasquale JA, Dezfuli BS. (2013). Local connected fractal dimension analysis in the gill of fish experimentally exposed to toxicants. Aquatic Toxicology. 175:12-9. https://doi.org/10.1016/j.aquatox.2016.03.011

[34] Martin JJ, Martin R, Codesal J, Fraile B, Paniagua R, Santamaria L. (2001). Cadmium chloride-induced dysplastic changes in the ventral rat prostate: an immunohistochemical and quantitative study. Prostate. 46(1):11-20. https://doi.org/10.1002/1097-0045(200101)46:1<11::aid-pros1003>3.0.co;2-k

[35] Moll R, Franke WW, Schiller DL, Geiger B, Krepler R. (1982). The catalog of human cytokeratins: patterns of expression in normal epithelia, tumors, and cultured cells. Cell. 31(1):11-24. https://doi.org/10.1016/0092-8674(82)90400-7

[36] Nagle RB, Ahmann FR, McDaniel KM, Paquin ML, Clark VA, Celniker A. (1987). Cytokeratin characterization of human prostatic carcinoma and its derived cell lines. Cancer Res. 47(1):281-6.

[37] Odgaard A and Gundersen HJ. (1993). Quantification of connectivity in cancellous bone, with special emphasis on 3-D reconstructions. Bone. 14(2):173-82. https://doi.org/10.1016/8756-3282(93)90245-6

[38] Oesterling JE. (1991). The origin and development of benign prostatic hyperplasia. An age-dependent process. J Androl. 12(6):348-55.

[39] Park Y, Lim S, Nam JW, Kim S. (2016). Measuring intratumor heterogeneity by network entropy using RNA-seq data. Sci Rep. 6:37767. https://doi.org/10.1038/srep37767

[40] Patel ND and Parsons JK. (2014). Epidemiology and etiology of benign prostatic hyperplasia and bladder outlet obstruction. Indian J Urol. 30(2):170-6. https://doi.org/10.4103/0970-1591.126900

[41] Plotnick RE, Gardner RH, Hargrove WW, Prestegaard K, Perlmutter M. (1996). Lacunarity analysis: a general technique for the analysis of spatial patterns. Phys Rev E. 53(5):5461–8. https://doi.org/10.1103/PhysRevE.53.5461

[42] Posadas AND, Giménez D, Quiroz R, Protz R. (2003). Multifractal Characterization of Soil Pore Systems. Soil Sci Soc Am J. 67(5):1361-9. https://doi.org/10.2136/sssaj2003.1361

[43] Quinlan RA, Schiller DL, Hatzfeld M, Achtstatter T, Moll R, Jorcano JL, et al. (1985). Patterns of expression and organization of cytokeratin intermediate filaments. Ann N Y Acad Sci. 455:282-306. https://doi.org/10.1111/j.1749-6632.1985.tb50418.x

[44] Rasband WS. (2012). ImageJ: Image Processing and Analysis in JAVA [Internet]. [Citado: 25 Junio 2024]. Disponible en: https://ui.adsabs.harvard.edu/abs/2012ascl.soft06013R/abstract

[45] Reljin IS and Reljin BD. (2002). Fractal geometry and multifractals in analyzing and processing medical data and images. Archive of Oncology. 10(4):283-93. https://doi.org/10.2298/AOO0204283R

[46] Santamaria L and Ingelmo I. (2023). Multifractal structure of cholinergic innervation in the tunica albuginea of rat testis. Comparison with different models simulating nerve networks. Open Access Research Journal of Life Sciences. 06(02):053-71. https://doi.org/10.53022/oarjls.2023.6.2.0069

[47] Santamaria L, Ingelmo I, Sinues B, Martinez L, Teba F. (2018). Quantification of the heterogeneity of cytokeratin 18 immunoexpression in prostate adenocarcinoma and normal prostate: Global and local features. Histol Histopathol. 33(10):1099-110. https://doi.org/10.14670/HH-18-009

[48] Santamaría L, Ingelmo I, Teba F. (2017). Structural Patterns of Immunoreactivity to Cytokeratin 18 in Normal Prostate and Benign Prostate Hyperplasia: Global and Local Differences. Open Journal of Pathology. 7(2):25-44. https://doi.org/10.4236/ojpathology.2017.72004

[49] Santamaría L, Ingelmo I, Teba F, Coloma A, Martínez L. (2016). Quantitative Stereological Estimations of Structural Patterns of the Glandular Tree in Benign Hyperplasia of Prostate. Open Journal of Pathology. 6(3):122-33. https://doi.org/10.4236/ojpathology.2016.63015

[50] Schlegel R, Banks-Schlegel S, Pinkus GS. (1980). Immunohistochemical localization of keratin in normal human tissues Lab Invest. 42(1):91-6.

[51] Sedivy R and Windischberger C. (1998). Fractal analysis of a breast carcinoma--presentation of a modern morphometric method. Wien Med Wochenschr. 148(14):335-7.

[52] Sijilmassi O, López Alonso JM, Del Río Sevilla A, Barrio Asensio MC. (2020). Multifractal analysis of embryonic eye tissues from female mice with folic acid deficiency. Part II: Local Connected Fractal Dimension Analysis. Chaos, Solitons and Fractals. 138:109887. https://doi.org/10.1016/j.chaos.2020.109887

[53] Sijilmassi Q, López Alonso JM, Del Río Sevilla A, Barrio Asensio MC. (2020). Multifractal analysis of embryonic eye structures from female mice with dietary folic acid deficiency. Part I: Fractal dimension, lacunarity, divergence, and multifractal spectrum. Chaos, Solitons and Fractals,. 138:109885. https://doi.org/10.1016/j.chaos.2020.109885

[54] Smith TG, Jr., Lange GD, Marks WB. (1996). Fractal methods and results in cellular morphology--dimensions, lacunarity, and multifractals. J Neurosci Methods. 69(2):123-36. https://doi.org/10.1016/S0165-0270(96)00080-5

[55] Sorensen FB. (1991). Stereological estimation of the mean and variance of nuclear volume from vertical sections. J Microsc. 162(Pt 2):203-29. https://doi.org/10.1111/j.1365-2818.1991.tb03132.x

[56] Spasic S, Kalauzi A, Kesic S, Obradovic M, Saponjic J. (2011). Surrogate data modeling the relationship between high-frequency amplitudes and Higuchi fractal dimension of EEG signals in anesthetized rats. J Theor Biol. 289:160-6. https://doi.org/10.1016/j.jtbi.2011.08.037

[57] Szczepaniak A and Macek WM. (2008). Asymmetric multifractal model for solar wind intermittent turbulence. Nonlin Processes Geophys. 5(4):615–20. https://doi.org/10.5194/npg-15-615-2008

[58] Teba F, Martín R, Gómez V, Herranz LM, Santamaría L. (2007). Cell Proliferation and Volume-Weighted Mean Nuclear Volume in High-Grade Pin and Adenocarcinoma, compared with Normal Prostate. Image Analysis and Stereology. 26(2):93-9. https://doi.org/10.5566/ias.v26.p93-99

[59] Tolkach Y and Kristiansen G. (2018). The Heterogeneity of Prostate Cancer: A Practical Approach. Pathobiology. 85(1-2):108-16. https://doi.org/10.1159/000477852

[60] Verhagen AP, Ramaekers FC, Aalders TW, Schaafsma H.E., Debruyne FM, Schalken JA. (1992). Colocalization of basal and luminal cell-type cytokeratins in human prostate cancer. Cancer Res. 52(22):6182-7.

[61] Voss RF and Wyatt JCY. (1993). Multifractals and the Local Connected Fractal Dimension. En: Crilly AJ, Earnshaw RA and Jones H, editors. Applications of Fractals and Chaos. Heidelberg, Berlin: Springer. pp:171-92.